University of New Hampshire
University of New Hampshire Scholars' Repository

Master's Theses and Capstones

Student Scholarship

Spring 2009

Amino acid paleothermometry in the Summer Lake basin, Oregon, using fossil ostracodes from the middle to late Pleistocene

Krista L. Reichert
University of New Hampshire, Durham

Follow this and additional works at: https://scholars.unh.edu/thesis

AMINO ACID PALEOTHERMOMETRY IN THE SUMMER LAKE BASIN,

OREGON, USING FOSSIL OSTRACODES FROM THE MIDDLE TO LATE

PLEISTOCENE

BY

KRISTA L. REICHERT

B.S., Skidmore College, 2002

THESIS

Submitted to the University of New Hampshire

in Partial Fulfillment of

the Requirements for the Degree of

Master of Science

in

Earth Sciences: Geochemical Systems

May, 2009

UMI Number: 1466949

INFORMATION TO USERS

The quality of this reproduction is dependent upon the quality of the copy submitted. Broken or indistinct print, colored or poor quality illustrations and photographs, print bleed-through, substandard margins, and improper alignment can adversely affect reproduction.

In the unlikely event that the author did not send a complete manuscript and there are missing pages, these will be noted. Also, if unauthorized copyright material had to be removed, a note will indicate the deletion.

UMI®
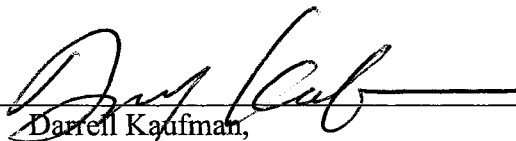
This thesis has been examined and approved.

Thesis Director, Joseph M. Licciardi,
Associate Professor of Earth Sciences

Darrell Kaufman,
Professor of Geology and Environmental Science
Northern Arizona University

William Clyde,
Associate Professor of Earth Sciences

5/8/09
Date

DEDICATION

This thesis is dedicated to my father whose love of science has been an inspiration to me.

ACKNOWLEDGEMENTS

TABLE OF CONTENTS

LIST OF TABLES

LIST OF FIGURES

ABSTRACT

AMINO ACID PALEOTHERMOMETRY IN THE SUMMER LAKE BASIN,

OREGON, USING FOSSIL OSTRACODES FROM THE MIDDLE TO LATE

PLEISTOCENE

by

Krista L. Reichert

University of New Hampshire, May 2009

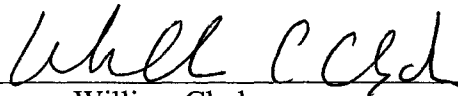Developing quantitative records that uniquely resolve past temperatures is important for interpreting regional paleoclimate changes. Here I analyze the extent of amino acid racemization in fossil ostracodes, and use a previously published expression to calculate effective diagenetic temperatures (EDTs) in the Summer Lake basin of south-central Oregon for time intervals bracketed between 208 ka, 180 ka, 74 ka, and present day. Geochronological control is provided by a published age-depth model for the Ana River section in the Summer Lake basin. Reverse-phase high performance liquid chromatography (HPLC) was used to measure the enantiomeric composition of aspartic and glutamic acids in *Candona* and *Limnocythere* ostracode valves collected from 33 sedimentary horizons within a ~15-m section of lake sediments exposed along the Ana River. An average of 9 replicate subsamples were analyzed for each sample, and the

relative difference in the rate of racemization in the two genera was quantified by analyzing multiple pairs from the same stratigraphic horizons. Between 208–180 ka (MIS 7-6), the EDT was 7.0 ± 2.6°C, which overlaps with the current mean annual temperature near the site (9.5°C). The EDT for the time interval between 180–74 ka (MIS 6–4) was -3.2 ± 1.3°C and from 74 ka to present the EDT was 2.7 ± 1.2°C. EDT estimates spanning the MIS 6-4 are unexpectedly low given that this interval encompasses the last interglaciation, and suggests that either the Ana River section age-depth model is inaccurate, or other factors in addition to temperature influenced the rate of racemization in the ostracode valves analyzed.

CHAPTER 1

INTRODUCTION

1.1 Project overview

Reconstructing paleoclimatic conditions both globally and regionally is valuable for establishing a baseline of natural climate variability during the Quaternary and for providing a foundation to better understand controlling mechanisms in the climate system. Although long records of trends in atmospheric temperature (Dansgaard et al., 1993; Petit et al., 1999; Jouzel et al., 2007) and global ice volume (Martinson et al., 1987; Lisiecki and Raymo, 2004) have been reconstructed for the Quaternary, there are comparatively few continuous, regional terrestrial climate records that span comparably long time periods (Coplen et al., 1994; Hovan et al., 1989; Chen et al., 1999; Brigham-Grette et al., 2007).

Pluvial lake records provide an excellent source of paleoclimate data in the interior western U.S. (e.g., Benson, 1999; Cohen, 2003) because lakes respond quickly to climate perturbations and preserve high-resolution climate records in their sediments and fossils. During the Pleistocene, the Great Basin of the Basin and Range province contained a series of large pluvial lake systems (Figure 1) that expanded and contracted with glacial-interglacial cycles in response to fluctuations in evaporation and precipitation (Mifflin and Wheat, 1979; Benson, 1999; Reheis, 1999).

1
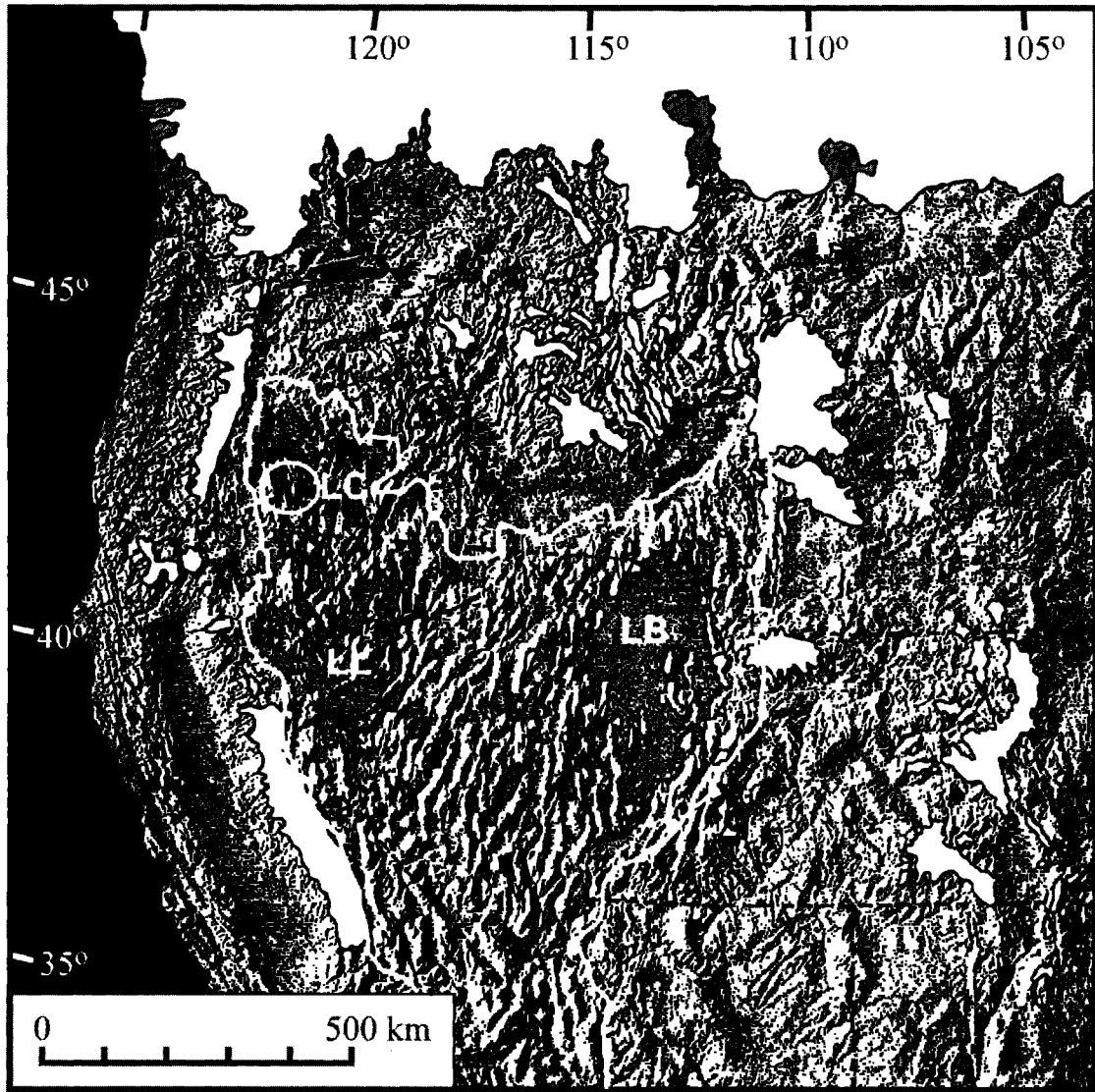
Figure 1: Digital elevation map of pluvial lakes and glaciers in the western U.S. Map shows glaciated areas (white) and maximum pluvial lake extents (blue) during the late Pleistocene. LC-Lake Chewaucan, LB-Lake Bonneville, LL-Lake Lahontan. Map compiled from Smith and Street-Perrott (1983), Negrini (2002), and Licciardi and Pierce (2008).

Some debate remains over whether pluvial lake-level fluctuations were solely the result of precipitation trends or if lake levels were influenced primarily by temperature-controlled evaporation (Cohen et al., 2000; Menking et al., 2004). The role of lower glacial-age temperatures on the hydrologic budget of these lakes is unresolved, due in large part to the limited number of temperature-specific paleoclimate proxies (e.g.,

2

Axford et al., 2009) that can be developed in terrestrial settings. Although proxies such as pollen, trace element ratios (e.g., Mg/Sr) and paleoecological reconstructions are to some degree dependent on temperature (Palacios-Fest et al., 1994; Klein et al., 1997), these indices can also be influenced by biological processes and other climate parameters such as precipitation, thus making it difficult to isolate the temperature effect.

Here, paleotemperature signatures are isolated from paleoprecipitation changes using an approach that relies on amino acid racemization (AAR) in fossils that have been independently dated (e.g., Oches et al., 1996), and that has only recently been applied to lacustrine ostracodes (Kaufman, 2003a). This study estimates paleotemperatures in the Summer Lake basin of south-central Oregon using the extent of AAR in fossil ostracodes during several intervals of the middle to late Pleistocene encompassing marine oxygen-isotope stages (MIS) 7 through 4. Ostracodes are bivalved microcrustaceans that are commonly used for a variety of terrestrial paleoclimate reconstructions because of their well-known environmental tolerance index and nearly ubiquitous preservation in lacustrine sediments (Delorme, 1969; Forester, 1983; Palacios-Fest et al., 1994). My specific strategy involves (1) estimation of temperatures during selected time intervals within the past 208 ka in the Summer Lake basin using AAR paleothermometry; (2) comparison of the AAR-based thermal history at Summer Lake to previous temperature estimates from Summer Lake and other pluvial lake systems in the Great Basin, and to regional western U.S. temperature trends during the middle to late Pleistocene; and (3) use of the Summer Lake AAR data to quantify the difference in the rate of racemization between two common ostracode genera, *Candona* and *Limnocythere*. Results from this project contribute to establishing an accurate Pleistocene thermochronology for the

3

northwestern portion of the Great Basin and provide insight on paleoenvironmental conditions in the western U.S.

1.2 Pluvial lake growth in the Great Basin

Throughout the Pleistocene and Holocene, the Great Basin held as many as 80 pluvial lakes which transgressed and regressed on centennial to millennial time scales (e.g., Mifflin and Wheat, 1979; Smith and Street-Perrott, 1983; Benson, 1999; Negrini, 2002; Cohen, 2003). These lake-level fluctuations are hypothesized to have been driven by diversion of winter storms toward the Great Basin, as the polar jet stream was shifted southward by the presence of the Laurentide Ice Sheet (Antevs, 1952; Benson and Thompson, 1987; Benson et al., 1996; Oviatt, 1997; Benson, 1999). This mechanism is supported by atmospheric general circulation model simulations (Manabe and Broccoli, 1985; Kutzbach and Guetter, 1986; Bartlein et al., 1998); however, alternative hypotheses have been advanced to explain the existence and growth of Pleistocene pluvial lakes. Stott et al. (2002) attributed lake growth throughout the Great Basin to intensified monsoon cycles under enhanced millennial-scale "super" El Niño-Southern Oscillation (ENSO)-like conditions. Other workers have hypothesized that correlations between the timing of Dansgaard-Oeschger events and pluvial lake fluctuations may reflect teleconnections between the North Atlantic and North Pacific on millennial and Milankovich time scales (Phillips et al., 1994; Clark and Bartlein, 1995; Benson et al., 1997a; Zic et al., 2002). However, these possible teleconnections are not fully resolved and complicated by probable variations in the intensity of teleconnections throughout space and time (Benson, 1999). Furthermore, lake highstands and lowstands were not synchronous throughout the Great Basin during the Pleistocene, and instead varied

4

regionally in their timing (Benson, 1999; Licciardi, 2001; Garcia and Stokes, 2006). This asynchrony may best be explained by synoptic-scale climate forcing, such as an enhanced monsoon, or variable hydrologic responses in different-sized basins (Licciardi, 2001).

1.3 Geological setting

The geology of the Summer Lake region was first described in detail by Russell (1884) and Allison (1940, 1982). The region is underlain by Tertiary basalt flows and mantled by Quaternary lacustrine and deltaic sediments and alluvium (Allison, 1982). Like other closed pluvial lake basins in the northwestern Great Basin, the Lake Chewaucan basin has been down-faulted and is characterized by tilted half-graben fault blocks (Pezzopane and Weldon, 1993). Modern-day Summer Lake is held in the largest of four sub-basins that comprise the pluvial Lake Chewaucan basin and is separated from the Lake Abert basin and the upper and lower Chewaucan Marsh sub-basins by an alluvial fan near the town of Paisley (Allison, 1982). (Figure 2). The site of this investigation is an exposed bluff of the Ana River (Figures 3 & 4), which is the only major river flowing into Summer Lake; the river is fed by subsurface springs which hydrologically connect the Summer Lake basin to the Silver Lake basin to the north (Allison, 1982).

5
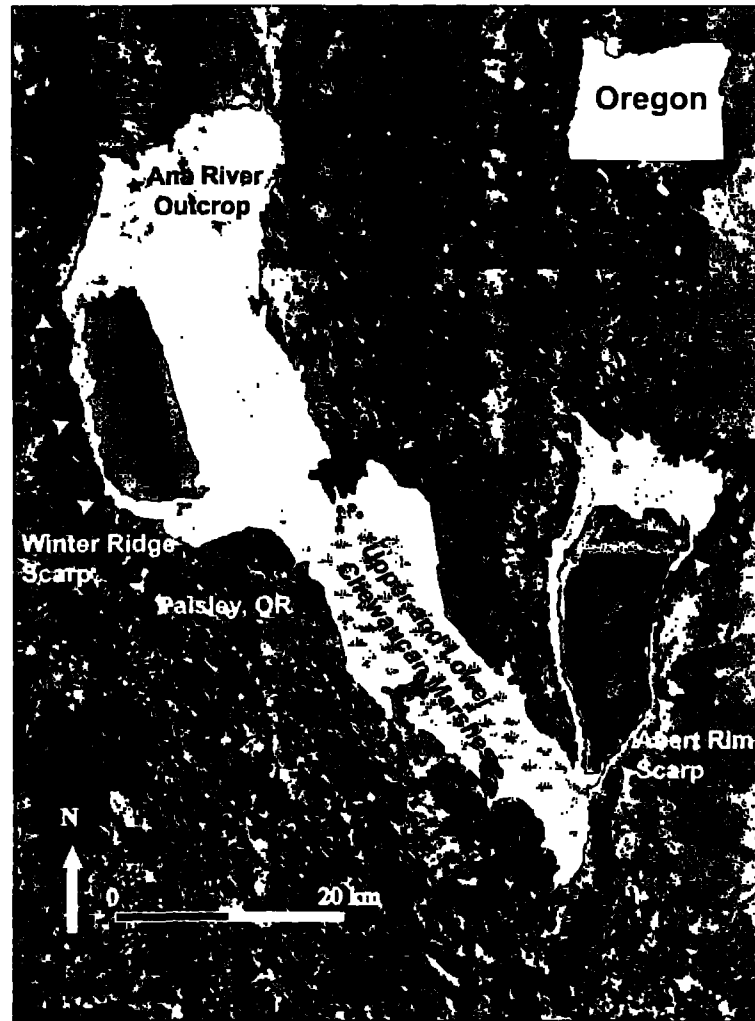
Figure 2: Map of pluvial Lake Chewaucan. The Lake Chewaucan basin is bound by the fault scarps Winter Ridge and Abert Rim, and is divided into four sub-basins. Light blue–maximum extent of pluvial Lake Chewaucan; dark blue–present-day Summer Lake and Lake Abert; red star–Ana River stratigraphic section. Background image from Google Earth.

The Ana River stratigraphic section has long been a centerpiece of Quaternary studies in the Great Basin because its well-exposed, fossil-rich sediments reveal one of the longest and most continuous sequences in North America. Stratigraphic investigations of the section (Allison, 1982; Davis, 1985) indicate continuous deposition over 200,000 years with the exception of a prominent unconformity marked by a 4-cm-thick lag deposit (Figure 3). This unconformity is interpreted to reflect a time of lake

6

desiccation and basin deflation during MIS 5e (Davis, 1985; Erbes, 1996; Negrini et al., 2000). In addition, Holocene sediments are missing from the top of the section due to considerable deflation of the modern basin surface (Negrini et al., 2000). Age control for the Ana River section is described in section 1.7.
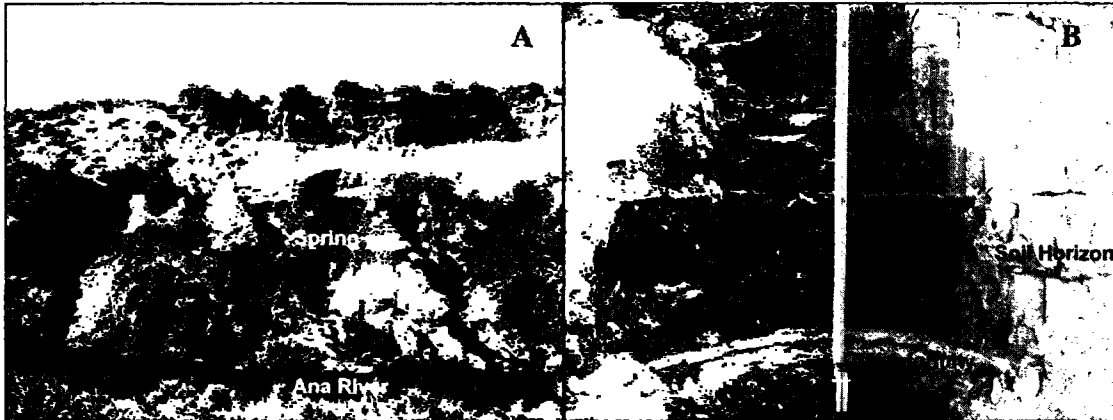
Figure 3: Photo of Ana River section and MIS 5e unconformity lag deposit. Panel A: View of the Ana River section. Top of the section is 1288 m in elevation. Panel B: Major unconformity corresponding to MIS 5e is marked by a thick lag deposit at the bottom of the photo.

1.4 Modern climate of Summer Lake

Climate data have been recorded by a National Weather Service station near the town of Summer Lake since 1957, including daily and monthly precipitation and temperature means and extremes. The modern climate of the Summer Lake basin is semi-arid (data available from Western Regional Climate Center, Desert Research Institute; www.wrcc.dri.edu) due to its location in the rain shadow of the Cascade Range. Modern mean annual temperature (MAT) is 9.5°C and provides a reference value for comparing paleotemperatures through time (Figure 4). Average annual pan evaporation from Summer Lake is 136.4 cm, and average annual precipitation is 32.1 cm (water equivalent). Winter snow accounts for most of the annual precipitation total, with summer months receiving less precipitation as a result of a northward shift of Pacific

7

storm tracks brought on by a suppression of westerly winds (Oregon Climate Service, Oregon State University, www.ocs.oregonstate.edu/index.html).
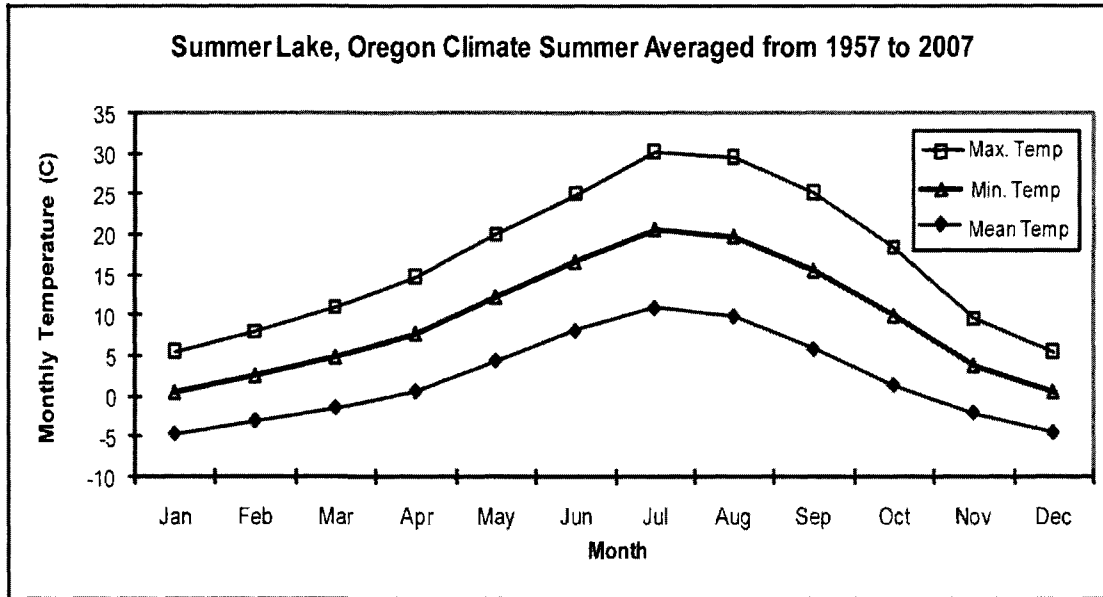
Figure 4: Mean monthly temperature extremes for the town of Summer Lake. Data from Western Regional Climate Center, Desert Research Institute.

1.5 Previous paleoclimate investigations in the Chewaucan Basin

Here I build upon previous paleoclimate investigations in the Chewaucan basin by Cohen et al. (2000) and Negrini et al. (2000). Proxies developed in the Chewaucan basin constrain a detailed paleoenvironmental record over the past 250 ka including evidence from ostracode assemblages, stable isotope and trace element concentrations measured on ostracode valves, magnetic susceptibility and grain size analyses measured in sediment, and palynology (Cohen et al., 2000; Negrini et al., 2000) (Figure 5). Much of the proxy data from the Ana River section rely on measurements in ostracode valves, which are ubiquitous throughout the entire section (Appendix B).

8
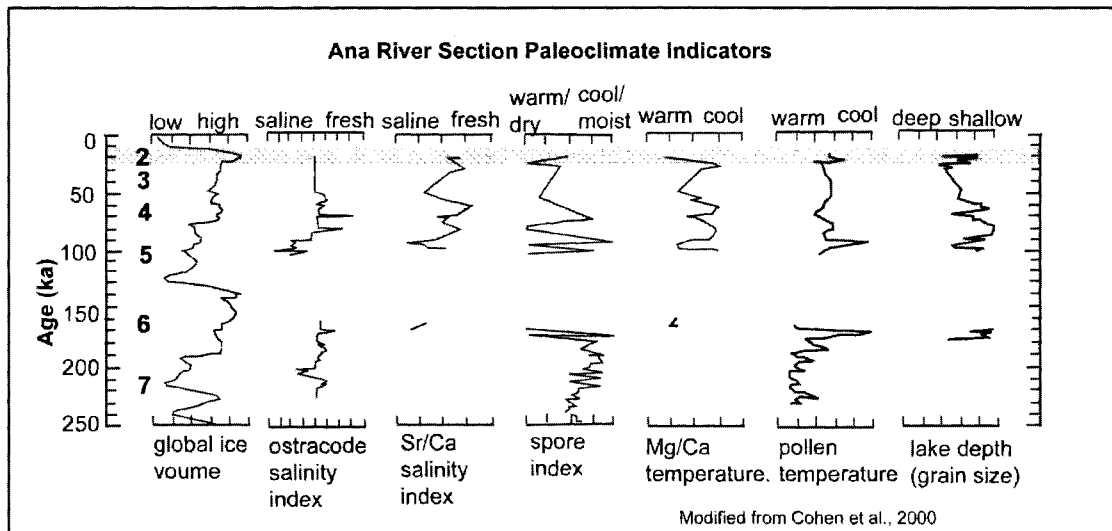
Figure 5: Ana River section paleoclimate indicators. From left to right: SPECMAP record of global ice volume (Martinson et al., 1987) and numbered MIS, with grey shaded areas corresponding to even-numbered MIS (glacial periods); paleosalinity index determined from ostracode paleoecology; Sr/Ca salinity index from measurements in ostracodes; spore index reflecting evaporation and precipitation; Mg/Ca water temperature record from measurements in ostracodes; and inferred air temperatures from pollen spore indices. Modified from Cohen et al. (2000) and references therein.

Paleotemperatures in the Lake Chewaucan basin have been estimated using palynology and Mg/Ca partitioning ratios in ostracodes (Palacios-Fest et al., 1994; Cohen et al., 2000). Pollen and spore index proxy records of terrestrial temperature indicate an overall decrease in air temperature from 230-160 ka. Mg/Ca and spore proxy data indicates cooling events occurring at the onset of MIS 4 (~75-60 ka) and MIS 2 (~25-19 ka). The water temperature signal from Mg/Ca partitioning in ostracode valves generally agrees with spore proxy data from ~100 ka to 20 ka; however, the temperature signal from pollen does not in agree with record from either of these proxies for this time interval. Although general temperature trends can be inferred from palynology and Mg/Ca, these proxies may also show the influence of other climate properties, such as precipitation, or from changes in lake water chemistry (Palacios-Fest et al., 1994).

9

Salinity proxy records generally track changes in the temperature record for the Ana River section, as colder temperatures result in reduced evaporation from the lake basin as a consequence of temperatures effect on vapor pressure (Cohen et al., 2000; Kaufman, 2003a). Paleotemperature estimates from this study are discussed in the context of other Summer Lake paleoclimate indices in Chapter 4.

1.6 Late Pleistocene temperature estimates in the western U.S.

Several quantitative and qualitative studies in the western U.S. constrain a range of middle to late Pleistocene temperatures that are between 4°C and 18°C cooler than modern MATs (Table 1). There is a paucity of paleotemperature records available for MIS 6 (Roberts et al., 1997; Quade et al., 2003; Kaufman, 2003a), and there are no terrestrial paleotemperature records from MIS 4. Evidence from halite fluid inclusions suggests that temperatures from 186 ka to 120 ka were 10-15°C cooler than modern MAT (Roberts et al., 1997), which is consistent with MIS 6 temperatures in southern Nevada that are 10.8°C cooler than modern MAT, as estimated using $\delta^{18}O$ values on ostracodes (Quade et al., 2003). These temperature depressions are in contrast with EDT estimates from the Lake Bonneville basin (Kaufman, 2003a) which suggest EDT since 620 ka is cooler than modern MAT by approximately 4.6°C. It important to note that paleotemperature estimates derived from $\delta^{18}O$ measured on ostracode valves (e.g., Quade et al., 2003) are more qualitative than estimates derived from halite fluid inclusion or amino acid paleothermometry, as the $\delta^{18}O$ record may also be a proxy for regional changes in precipitation and runoff (Klein et al., 1997).

With the exception of temperature depressions estimated by Clark and Bartlein (1995), discrepancies between last glacial maximum (LGM) temperature depression

10

estimates across the western U.S. are relatively small, and may reflect differences in site elevation, latitude, and proxy methods used. This study extends the geographic coverage of terrestrial temperature estimates in the western U.S. and provides critical new constraints on temperature depressions.

Location	Proxy	Reference	Temp Depression (°C)	Time Interval (ka)
Lake Bonneville	AAR	Kaufman, 2003a	4.6	620-150
southern Nevada	$\delta^{18}O$ in ostracodes	Quade et al., 2003	10.8	186-130
Death Valley	halite fluid inclusion	Roberts et al., 1997	10-15	186-120
Lake Estancia	hydrologic modeling	Brakenridge, 1978	7-8	21 (LGM)
southern Nevada	$\delta^{18}O$ in ostracodes	Quade et al., 2003	5.6	21 (LGM)
Uinta & Wasatch Mts.	ELA reconstructions	Laabs et al., 2005	6-7	21 (LGM)
Yucca Mt	packrat middens	Thompson et al., 1999	7.5	21 (LGM)
Western U.S.	ELA reconstructions	Clark and Bartlein, 1995	8-18	21 (LGM)
Great Basin	nivation features	Dohrenwend, 1984	7	21 (LGM)
Colorado Plateau	pollen	Anderson et al., 2000	5	21 (LGM)
Lake Estancia	hydrologic modeling	Menking et al., 2004	~5	21 (LGM)
Lake Bonneville	AAR	Kaufman, 2003a	10	24-12

Table 1: Paleotemperature depression estimates in the western U.S. Estimates are listed from oldest to youngest. Temperature depressions estimated using AAR are with respect to modern mean annual temperatures of 9.4°C and 9.5°C in the Bonneville and Summer Lake basins respectively. ELA–equilibrium line altitude.

1.7 Geochronology

Previous workers have described the stratigraphy, paleomagnetism, and ostracode paleoecology of the Ana River section (Allison, 1982; Davis, 1985; Palacios-Fest et al., 1993; Erbes, 1996; Cohen et al., 2000). Age control for the section (Table 2) is based on [14]C (Davis, 1985), tephrochronology, thermoluminescence (TL), K-Ar tephra correlation (Davis, 1985; Berger, 1991; Herrero-Bervera et al., 1994; Benson et al., 1997b; Kuehn and Foit, 2007) and correlation of paleomagnetic secular variation (PSV) with the Mono Lake and Pringle Falls excursions (Negrini et al., 1988; Negrini and Davis, 1992; Negrini et al., 2000). Most dated horizons are above the major unconformity at 5.12 m depth,

11

whereas ages below this unconformity are less well-constrained. This study uses the age-depth model (Figure 6) developed by Negrini et al. (2000)
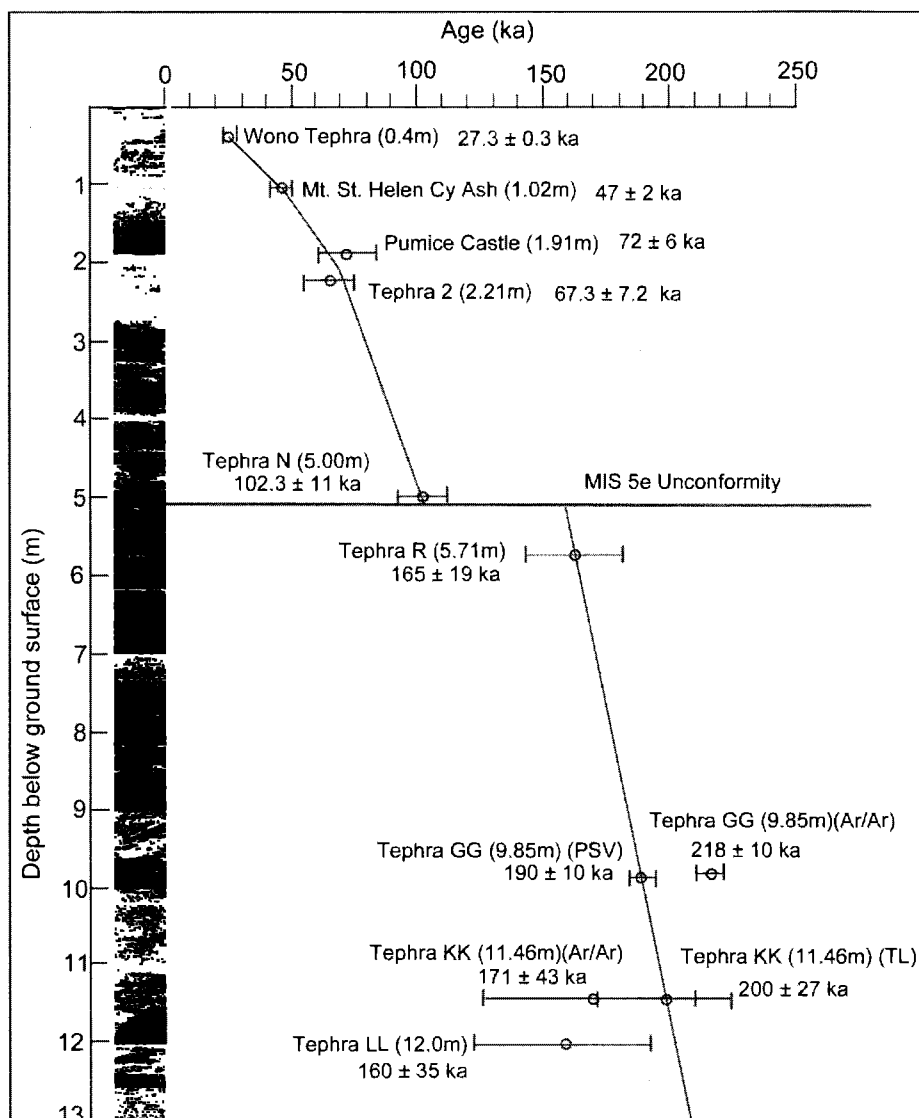
Figure 6: Age-depth model for the Ana River section. Model follows Negrini et al. (2000). The age-depth trend below the unconformity is fit to the TL ages of Tephra R and Tephra KK, which are assumed to be reliable, and the shaded region along the age-depth line represents the uncertainty. Stratigraphic section photo-log along the right side of the figure is shown in more detail in Appendix C including depths of each sample. Depths of dated ashes correspond to stratigraphic measurements from this study. Equations used to interpolate sample ages are as follows, where y is age (ka) and x is depth (m): (1) depth interval 0.40–1.02 m; y = 23.08x + 18.39; (2) depth interval 1.02–2.21 m; y = 21.63x + 24.93; (3) depth interval 2.21–5.00 m; y = 11.05x + 46.73; (4) depth below the unconformity; y = 6.49x + 125.97.

12

This age-depth model is favored over other possible age-depth models because it has been used as the chronological basis for multi-proxy paleoenvironmental records from Summer Lake over the past 250,000 years (Figure 5), thereby ensuring a direct comparison of paleotemperatures derived here to published estimates of temperature trends in the basin (Cohen et al., 2000; Negrini et al., 2000).

Depth (m)	Horizon	Age (ka)	Method
0.40	Wono Tephra	27.3 ± 0.3	radiocarbon[1]
1.02	Mt. St. Helens Cy ash	47 ± 2	TL[2]
1.91	Pumice Castle	72 ± 6	K-Ar[3,4]
2.21	Tephra 2	67.3 ± 7.2	TL[2]
5.00	Tephra N	102.3 ± 11	TL[2]
5.71	Tephra R	165 ± 19	TL[2]
9.85	Tephra GG	$190 \pm 10, 218 \pm 10$	PSV[5], Ar/Ar[6]
11.46	Tephra KK	$171 \pm 43; 200 \pm 27$	TL[2], Ar/Ar[6]
12.00	Tephra LL	160 ± 35	TL[2]

Table 2: Age control for the Ana River section. Published ages from tephrochronology and correlated PSV correlation are based on Negrini et al. (2000). Our study follows Negrini et al. (2000) and employs 190 ± 10 ka and 200 ± 27 as the ages of Tephra GG and Tephra KK, respectively. References are: 1) Benson et al., 1997b; 2) Berger, 1991; 3) Davis, 1985; 4) Bacon, 1983; 5) Negrini, 2000; 6) Herrero-Bervera et al., 1994.

Uncertainty in the Negrini et al. (2000) age-depth model arises from errors associated with each individual age determination used to construct the model. Although there are conflicting age estimates and apparent stratigraphic age reversals below the unconformity, all tephra ages below the unconformity agree within error of the preferred age-depth model (Negrini et al., 2000). The linear portion of the age-depth model is anchored to in-situ TL ages estimates for Tephra R and Tephra KK, which are considered reliable (Berger, 1991). The TL age estimate of Tephra LL is not reliable; however, because of abnormal TL systematics in this sample (Berger, 1991). This study employs an age of 190 ± 10 ka for Tephra GG following Negrini et al. (2000). The occurrence of Tephra GG in the Summer Lake basin has been correlated to Tephra D at Pringle Falls,

Oregon, which has an Ar/Ar age of 218 ± 10 ka (Herrero-Bervera et al., 1994). However, Negrini et al. (2000) ascertained that the tephra correlation age is overestimated as evidenced by a geomagnetic excursion measured on similar aged sediments as Tephra D that correlates to a paleomagnetic intensity low in marine sediment worldwide and has a radiometric age of 190 ± 10 ka dated in the North Atlantic (Henyey et al., 1995).

This study estimates ages of each sampled horizon by linear interpolation from the Negrini et al. (2000) age-depth model. Following Negrini et al. (2000), an uncertainty of ±23 kyr is assigned to all samples below the unconformity (Figure 6), as constrained by uncertainties of the TL age measurements for Tephra R and Tephra KK (Berger 1991). Above the unconformity, sample age uncertainty estimates were determined by interpolation between measured tephra age uncertainties for and the stratigraphic positions of each dated tephra layers (Negrini et al., 2000 and references therein).

CHAPTER 2

METHODS

2.1 Site stratigraphy

A stratigraphic sequence along a north-facing cut bank of the Ana River corresponding to outcrop E of Davis (1985) at 42°59.543'N, 120°44.635'W was photo-logged and described in centimeter detail to a depth of 13.0 m below the top of the section (Appendix C). Field descriptions of sediments and tephras were supplemented by field notes taken by J.O. Davis (unpublished, 1985) and J.M. Licciardi (unpublished, 1993), but ongoing bank erosion prevented examination of the exact bluff face stratigraphy described by Davis and Licciardi. Nevertheless, stratigraphic correlation of distinctive tephra layers and sedimentary horizons to the unpublished descriptions of Davis and Licciardi, with only minimal offsets, adds confidence to the chronostratigraphy for this study, as all described tephras from our stratigraphic investigation were positively identified and correlated to named and described tephras (Table 2).

A total of 101 sediment samples spanning the uppermost 13 m of the 15-m-high exposure were collected from discrete sediment horizons in centimeter-scale intervals, based on the occurrence and preservation of ostracodes and changes in stratigraphy (Figure 7). Because amino acid paleothermometry relies on accurate chronostratigraphy, a strong effort was made to collect samples from layers close to dated tephras.

15
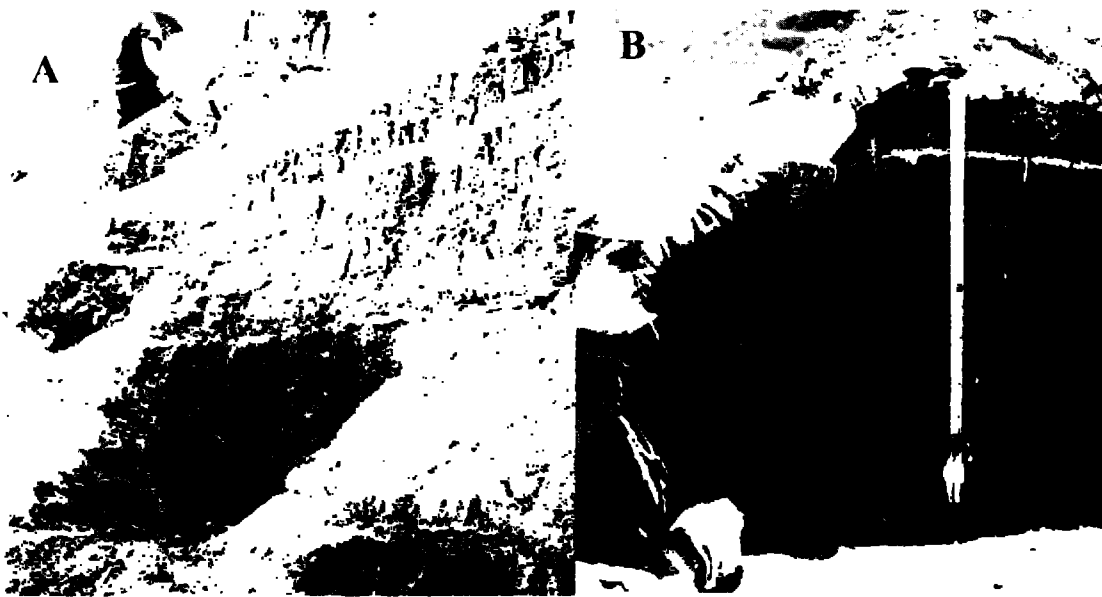
Figure 7: Photo of field sampling and photologging. Panel A: Field description and collection of sediment samples from the Ana River section bluff (sample collection methods detailed in Appendix A); Panel B: Example of sediment photo logging.

2.2 Principles of amino acid paleothermometry

The basic principles of amino acid racemization and paleothermometry are well documented in the literature (e.g., McCoy, 1987; Miller and Brigham-Grette, 1989) and described here briefly. Amino acids in all organisms exist as mirror-image enantiomers with identical chemical properties. Most living organisms utilize only L-form (*levo*) enantiomers, and upon death the process of racemization inverts these to D-form (*dextro*) enantiomers. The extent of racemization of a particular amino acid preserved in fossilized remains is measured as the ratio of D/L enantiomers and is dependent on both time elapsed since death and temperature (Schroeder and Bada, 1976). Because the temperature sensitivity of the racemization reaction can be described by the Arrhenius equation, D/L can be used either to date samples assumed to have experienced a constant burial temperature, or conversely to reconstruct the thermal history of a region if independent sample ages are known (Miller and Brigham-Grette, 1989). Because

16

racemization rates increase exponentially with rising temperature, a given amount of time a sample experiences at a high temperature is more significant to increasing D/L than an equal amount of time spent at a low temperature (Wehmiller, 1978).

This study uses an application of amino acid paleothermometry developed by Kaufman and Manley (1998) and modified by Kaufman (2000), which allows D/L measurements in extremely small samples. The temperature dependency of racemization has been established for modern and fossil ostracodes (Figure 8), allowing the effective diagenetic temperature (EDT) to be determined using an empirical power-law model and Arrhenius equation (Kaufman, 2003a). The EDT represents the integrated temperature experienced by a fossil since the death of an organism, and is therefore is not a measure of instantaneous temperature. This study estimates EDT as both the integrated temperature for the full duration a sample has been buried (T_{t1}, equation 1), and also estimates EDT for an interval of time between two samples of known age ($T_{(t2-t1)}$, equation 2). The value denoted by ΔT (equation 3) is the difference in EDT between the bracketed time interval ($T_{(t2-t1)}$) compared with the EDT since the younger sample was buried (T_{t1}). EDT equations 1 and 2 were derived by combining the Arrhenius equation, $k = Ae^{(-Ea/RT)}$ with an empirical power law model, as described in Kaufman (2000), $(1 + K')kt + C = [(1 + D/L)/(1 - K'D/L)]^n$. Figure 8 shows the modeled solution to equation 1.

$$T_{t1} = Ea / R\ell n[(1 + D/L)/(1 - K \times D/L)]^n - C/2At \qquad \textbf{(EQ 1)}$$

$$T_{(t_2-t_1)} = Ea / R\ell n(A[(t_2 - t_1)/(k_2 t_2 - k_1 t_1)]) \qquad \textbf{(EQ 2)}$$

$$\Delta T = T_{(t2-t1)} - T_{t1} \qquad \textbf{(EQ 3)}$$

17

where:

T_{t1} = EDT since t_1 (°C)

Ea = Ea the activation energy, 29.5 ± 0.2 (kcal mol^{-1}) for Asp and Glu

R = gas constant (0.001987 kcal K^{-1} mol^{-1})

D/L = racemization extent in analyzed sample

K = equilibrium constant (1.0)

n = 3.6 for Asp and 3.8 for Glu

C = 0.6 for Asp and 0.4 for Glu

A = frequency factor, 44.270.2 yr^{-1} for Asp and 42.370.2 yr^{-1} for Glu

$T_{(t2-t1)}$ = EDT for the interval of time between t_2 and t_1 (°C)

t_1 = age of the younger sample (ka)

t_2 = age of the older sample (ka)

k_1 = rate constant for the younger sample calculated using the power-law model

k_2 = rate constants for the older sample calculated using the power law model developed
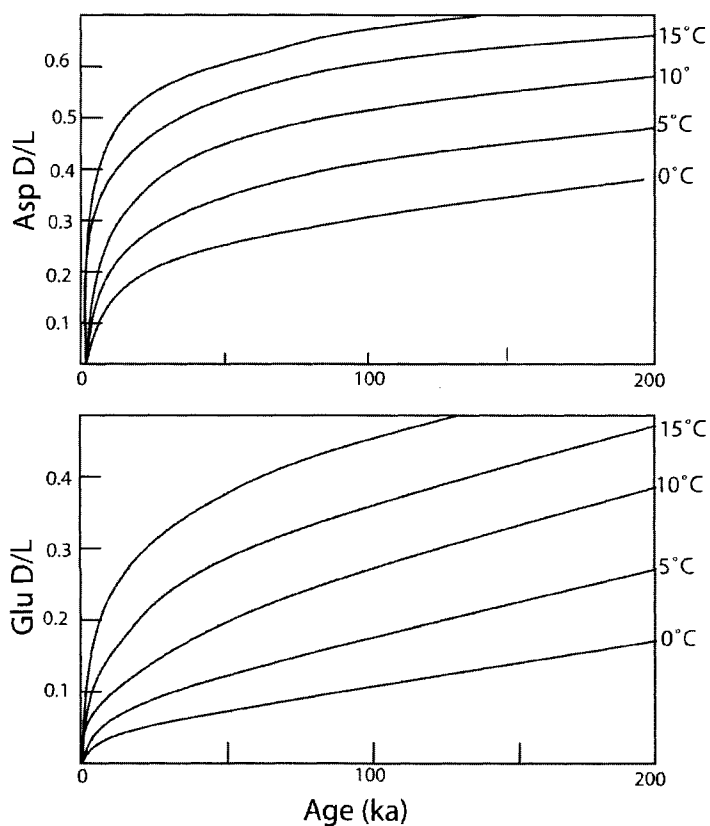
Figure 8: Racemization extent versus time and temperature. Figure shows modeled relation between extent of racemization (D/L of aspartic and glutamic acid) and sample age in *Candona* ostracodes under a range of temperatures. From Kaufman (2003a).

Additionally, EDT is not a long-term mean temperature and always overestimates

actual long-term mean temperature. For example, as shown in Figure 9 (Miller and

18

Clark, 2007), if a sample experienced a constant temperature of 20°C for the first half of its burial history and 0°C for the second half, the arithmetic mean temperature of 10°C during this interval of time corresponds to an EDT of 16.7°C for that same time interval, as a consequence of the exponential sensitivity of racemization rate to temperature. Because EDT is neither an instantaneous estimate nor arithmetic mean paleotemperature, caution must be exercised when comparing EDT results with instantaneous paleotemperatures and temperature depressions.

25

20

$T_1 = 16.7°C$

Temperature °C

15

10

Mean
temperature

5

0

Modified from Miller and Clark, 2007

-5

0   1   2
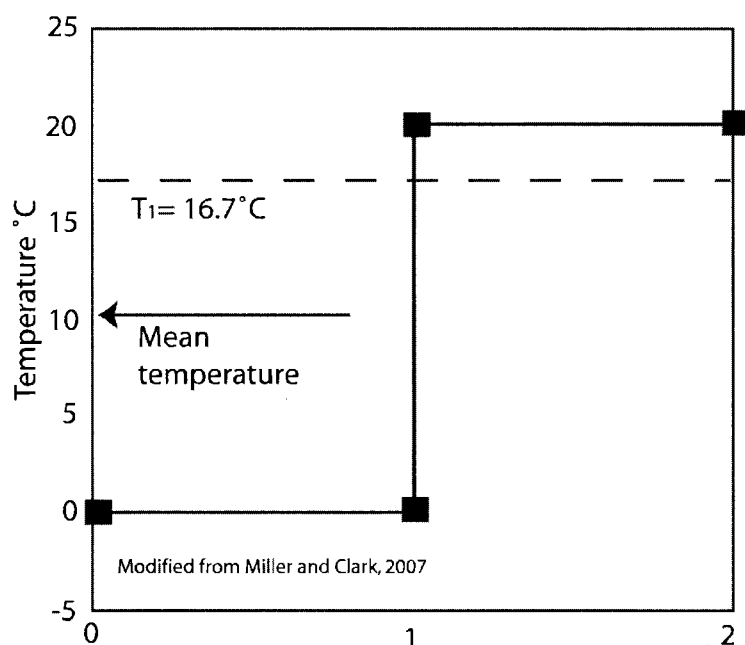
Figure 9: EDT versus mean temperature. This cartoon modified from Miller and Clark (2007) illustrates the difference between EDT and arithmetic mean temperatures, where as EDT is always higher because of the exponential relationship between racemization rate and temperature.

EDTs from the Summer Lake basin are estimated from the racemization extent of aspartic and glutamic acid (hereafter Asp and Glu, respectively) measured in two ostracode genera, *Candona* and *Limnocythere*. Asp and Glu D/L values are used because they elute quickly using reverse-phase HPLC and have successfully been utilized to

estimate EDTs in other lake basins in the western U.S. (Kaufman, 2003a). EDTs are reported here independently for Asp and Glu and also as weighted means of combined Asp and Glu EDT values.

2.3 Analytical methods

Ostracode valves from 33 sediment horizons were isolated for analysis at the University of New Hampshire by wet sieving of bulk sediment samples through a 150 μm mesh sieve and hand-picking the best preserved ostracode valves (see Appendix A for details). Samples were pretreated prior to sieving to deflocculate fine particles by freeze-thawing and stirring of a mixture of raw sediment, sodium hexametaphosphate, sodium bicarbonate, and water. Evidence of valve reworking or alteration was assessed under a microscope during hand-picking and includes but is not limited to discoloration, fragmented valves, concentrations of only adults or only juveniles, presence of ooids, oxidized valves, and in-filled valves.

Four species of ostracodes identified in previously published work (Palacios-Fest et al., 1994) were sampled at various stratigraphic depths in the Ana River section including *Candona caudata*, *Candona patzcuaro*, *Limnocythere ceriotuberosa*, and *Limnocythere sappaensis*. Two examples of unidentified monospecific *Candona sp.* were also identified by Jordon Bright at the Northern Arizona University Amino Acid Geochronology laboratory, who completed the ostracode identification for samples analyzed in this study. Although this study adopts the *Candona* taxonomic identification previously published for the Ana River section by Palacios-Fest et al. (1994), morphologic features observed in *Candona* throughout the Ana River section suggest a possibility that neither *C. caudata* nor *C. patzcuaro* are present in my samples (J. Bright,

20

personal communication, 2009), and that these ostracodes are more likely to be other species of *Candona*. Photos of *Candona* and *Limnocythere* from the Ana River section are presented in Appendix B.

Ostracode samples from each sediment horizon were subdivided into 8 to 10 sub-samples depending on the species and each sub-sample was analyzed independently. Because adult *Candona* are larger than adult *Limnocythere*, each sub-sample consisted of either one *Candona* valve or two *Limnocythere* valves.

All amino acid measurements were conducted at the Northern Arizona University Amino Acid Geochronology Laboratory in Flagstaff, Arizona. Ostracode valves were prepared and analyzed using methods developed by Kaufman and Manley (1998) with modifications for microfossils described by Kaufman (2000) (see Appendix A for details). Valves were cleaned by gentle sonication in distilled water followed by soaking for 2 hours in 3% hydrogen peroxide. Each valve (or two valves for *Limnocythere)* was placed in a separate sub-sample micro-reaction vial and hydrolyzed in 6M HCl under nitrogen for 6 hr at 110°C. The hydrolyzed samples were then rehydrated in 10 μM HCl prior to analysis on a Hewlett Packard HP1100 liquid chromatograph. Analytical precision for this method is 1-5% (Kaufman and Manley, 1998) and analytical uncertainty was determined by running sample blanks for this study along with regular assessment of RP-HPLC drift using ILC samples (Wehmiller, 1984) for inter-laboratory comparisons (Kaufman and Manley, 1998). Serine (Ser) concentrations in sample blanks were low, indicating that contamination by modern amino acids is negligible.

Pre-column derivatization was achieved on-line by auto-injecting samples with *o*-phthaldialdehyde (OPA) and N-isobutyryl- L-cysteine (IBLC). *D-* and *L*-form amino

acids were separated using a reverse-phase column packed with a C_{18} stationary phase by auto-injecting a linear gradient of eluents A (aqueous sodium acetate), B (methanol), and C (acetonitrile) through the column. Peaks in the fluorescence signal for each amino acid derivative were detected and integrated into D/L values by the HP Chemstation computer software.

2.4 Data screening and EDT estimation

2.4.1 Data quality analysis

In total, D/L values were measured in 479 ostracode sub-samples, including 91 *Candona caudata*, 139 *Candona patzcuaro*, and 249 *Limnocythere ceriotuberosa*. The extent of racemization for both Asp and Glu are reported for each taxon as the mean D/L of all sub-samples from each horizon; the $\pm1\sigma$ uncertainty therefore represents the inter-valve variability within a sample (Appendix D, Table A1). To reduce uncertainty in the EDT calculations, D/L data were screened by the methods described below.

The abundance of Ser was used to identify sub-samples with unexpectedly high concentrations of this labile amino acid. Sub-samples were rejected if the abundance ratio of Ser/Asp exceeded 2σ of mean sample Ser/Asp values. Outliers in the data were further revealed by scatter plots of all sub-sample Asp D/L vs. Glu D/L. Individual sub-sample D/L values were excluded from EDT analysis if their value exceeded $\pm2\sigma$ of the mean of all sub-samples for the entire sample after removing other aforementioned outliers. This screening resulted in rejection of 16.4% of the 479 subsamples (Figure 10) which compares with a data rejection rate of approximately ~12% of AAR data from the Lake Bonneville basin (Kaufman, 2003a). Furthermore, although D/L was measured in

22

Limnocythere sappaensis and the monospecific *Candona sp.* sub-samples, these D/L values were not used to calculate EDT because these species were each found in only a single sediment horizon. The mean D/L value for each sample was calculated using all sub-samples following data screening.
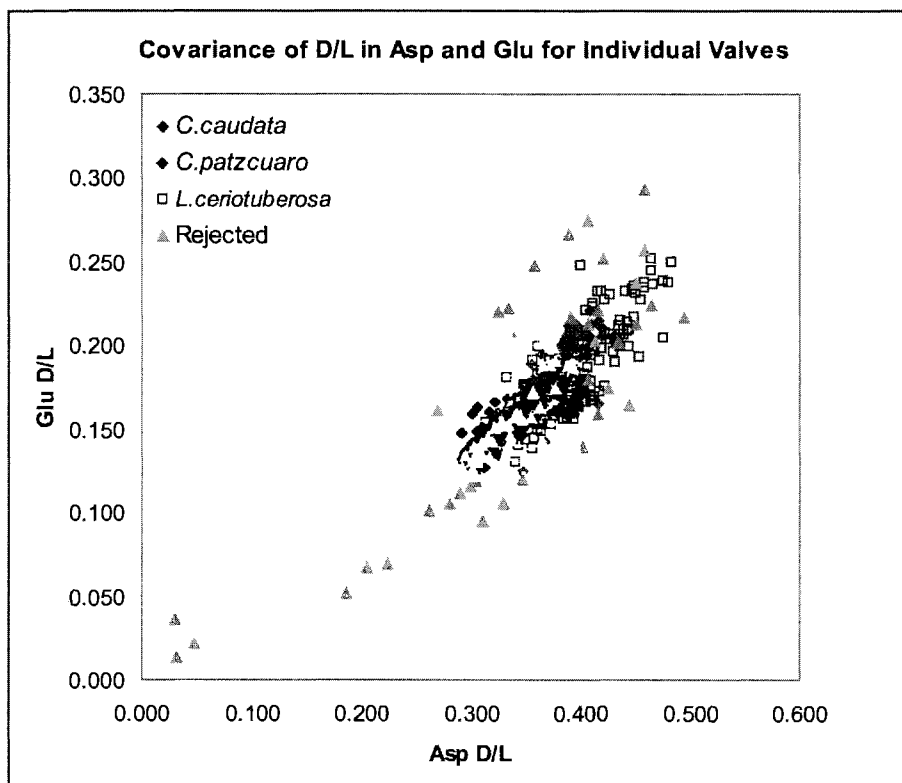
Figure 10: Covariance of D/L in aspartic and glutamic acids. All ostracode sub-samples are plotted as the covariance between D/L in aspartic (Asp) and glutamic (Glu).

2.4.2 Assessing taxonomic effects

Amino acid arrangement and bonding in a protein structure is dependent on the taxonomy of an organism, hence different taxa can experience different racemization rates (Wehmiller, 1993). Direct comparison of D/L results between different genera (and possibly species) of coeval ostracodes is therefore not possible unless the relative rates of racemization are known (Miller and Brigham-Grette, 1989). This study uses D/L values

to reconstruct paleotemperatures using both *Limnocythere,* the dominant ostracode genus in the Ana River section (Appendix B), and *Candona.* Previous EDT reconstructions in the Great Basin have relied exclusively on *Candona* (Kaufman, 2003a), given that *Limnocythere* has not been directly calibrated for amino acid paleothermometry.

Following Kaufman (2003a), I examined potential taxonomic differences between D/L values for *Candona* and *Limnocythere.* The ratios of $D/L_{Candona}$ to $D/L_{Limnocythere}$ were compared for 16 pairs of the two taxa from the same sediment horizons (Appendix D, Table A2). Because *Limnocythere* lacks a direct calibration for thermal reconstructions using AAR, this study normalizes *Limnocythere* D/L values to *Candona* D/L using the slope of a least-squares regression (Figure 12) of $D/L_{Candona}$ vs. $D/L_{Limnocythere}$ prior to EDT calculation.

The taxonomic difference between the two *Candona* species, *C. caudata* and *C. patzcuaro,* is expected to be minimal compared with the difference between *Candona* and *Limnocythere* genera. For all 3 instances of co-occurring *C. caudata* and *C. patzcuaro* samples, mean D/L were found to overlap within 1σ, indicating that species-related differences in D/L are negligible for *Candona* in the Ana River section.

EDT was calculated using the mean sample D/L for a given age (see section 3.2), and equations 1 and 2. Arrhenius parameters used for the EDT calculations were determined in heating experiments by Kaufman (2003a). All EDTs were calculated from Asp and Glu independently and also as the mean of combined Asp and Glu EDTs, which is weighted b y the in v rse of the variance EDT and σ. A Monte Carlo simulation developed by Darrell Kaufman was used to derive uncertainties in EDTs calculated from D/L and independent age inputs by integrating the inter-related errors of input Arrhenius

parameters as well as uncertainties in D/L values and ages over 5000 iterations (Kaufman, 2003a).

CHAPTER 3

RESULTS

3.1 Extent of racemization

Following stratigraphic expectations, ostracodes from the Ana River section show an overall increase in D/L with increasing depth in the section for both Asp and Glu (Figure 10, also Appendix D, Table A.1). Generally, there is more variability among inter-sample D/L values for *Limnocythere* data than for *Candona* (Appendix C, Table A.1). Above the unconformity, Asp D/L values in *Candona* range from 0.302 to 0.322 and from 0.136 to 0.153 for Glu. Below the unconformity, *Candona* Asp D/L values range from 0.343 to 0.402 and Glu D/L range from 0.158 to 0.208. Most minor stratigraphic reversals in the D/L data are less than 1σ of the mean of the next stratigraphically deeper sample, and are considered insignificant. The only samples that exhibit stratigraphic reversals $>1\sigma$ are AR07-4 and AR07-6, collected from 0.48 and 0.67 m depth, respectively, and samples collected from within 1 m of the unconformity (AR07-51, AR07-66 and AR07-69).

Of the 16 co-occurring samples of *Limnocythere* (all *ceriotuberosa*) and *Candona* (both *patzcuaro* and *caudata*) analyzed for taxonomic effects, *Limnocythere* have higher Asp D/L in all 16 samples, and higher Glu D/L in 14 of the 16 samples (Appendix C, Table A.1). The average the ratio of D/L$_{Candona}$ to D/L$_{Limnocythere}$ is 0.909 ± 0.047 for Asp

26

and 0.936 ± 0.068 for Glu. These relationships were used to normalize the D/L values

for *Limnocythere* to *Candona* D/L values using the slopes of the $D/L_{Candona}$ vs.

$D/L_{Limnocythere}$ regressions (Figure 11). Table A.1 in Appendix D shows all adjusted

Limnocythere D/L values used in EDT calculations. Uncertainty in the regression model

used to normalize *Limnocythere* D/L data is ±0.010 for Asp and ±0.08 for Glu based on

1σ of the co-occurring samples.
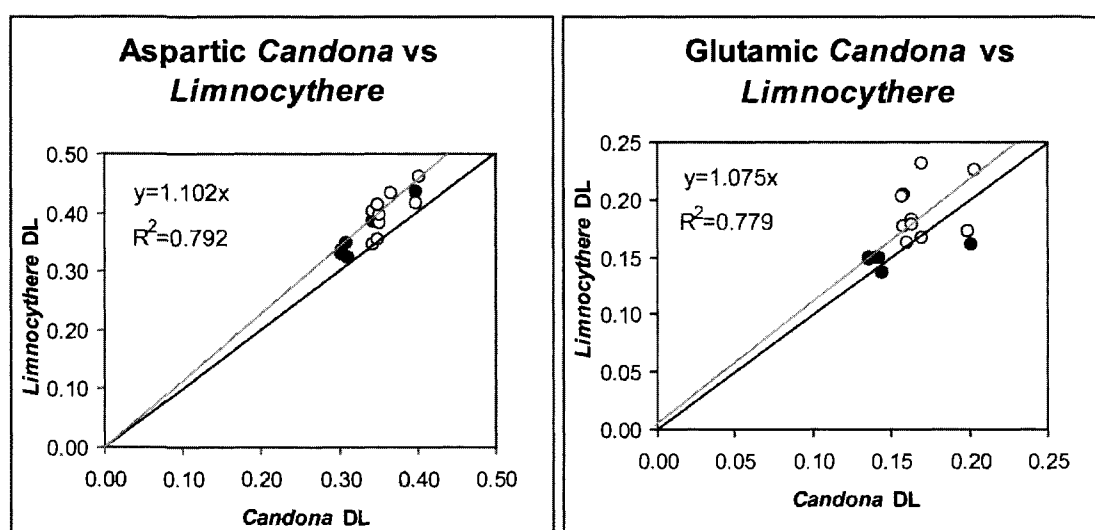
Figure 11: Taxonomic effects on *Candona* vs. *Limnocythere* D/L values. Plots show difference in the extent of racemization in 16 coeval samples of *Candona* and *Limnocythere* from the Ana River section. *Candona caudata* and *Candona patzcuaro* samples are shown as closed and open symbols, respectively. The linear relationship shown by the thin gray line is a 1:1 ratio of D/L values for Asp and Glu. Error bars represent ±1σ intra-sample variation. Data are listed in Table A.1.

3.2 EDT estimation models

The EDT was estimated based on D/L values representative of specific ages, which were calculated using three different approaches applied to the screened *Candona* and normalized *Limnocythere* D/L data. First, by combining *Candona* and adjusted *Limnocythere* D/L data, it is evident there are three "clusters" of D/L values (Figure 12) at 208 ka, 180 ka, and 74 ka. The weighted mean D/L value for each cluster was

27

determined by weighting each individual sample D/L value in the cluster by the inverse of its variance. Weighted mean ages for each cluster were determined by weighting each sediment horizon age in the cluster by the inverse of its variance as estimated from linear interpolation of the age uncertainties in the Negrini et al. (2000) age-depth model. A sample was included in a cluster if its mean D/L value did not show a reversal greater than 1σ with respect to the next-deepest sample in section. The number of samples included in each cluster ranges from 5 to 16 and a student t-test confirms that each data cluster is statistically distinguishable with respect to other clusters.
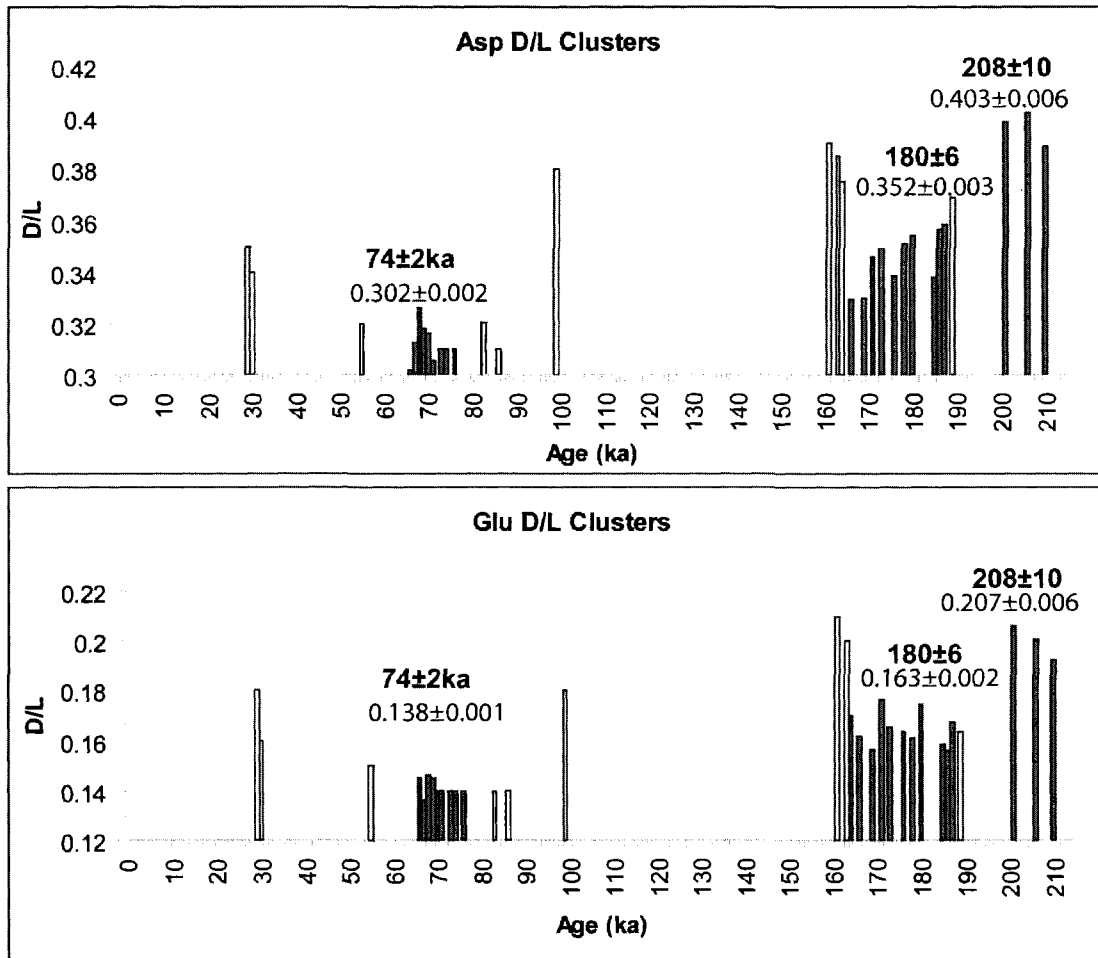
Figure 12: Histogram of D/L data clusters. Histogram shows distribution of clustered data in blue. White bars indicate sample data not included the data clusters. All normalized *Limnocythere* and *Candona* D/L values have been averaged to create the histogram.

28

As two alternatives to the cluster approach, mean EDT estimates were determined from a least-squares linear regression of D/L vs. age for all samples throughout the section (Figure 13), and from a compound linear regression of D/L vs. age, which considers sample data obtained above and below the unconformity separately (Figure 14). Regression-derived ages for both regression models were the same as for mean ages identified by the cluster approach, which allows EDT estimates from these three methods to be compared directly (see Table 3).

Simple Linear Regression of D/L vs. Age

$$Asp = 0.0005x + 0.2698$$
$$R^2 = 0.5838$$

$$Glu = 0.0003x + 0.1176$$
$$R^2 = 0.4765$$
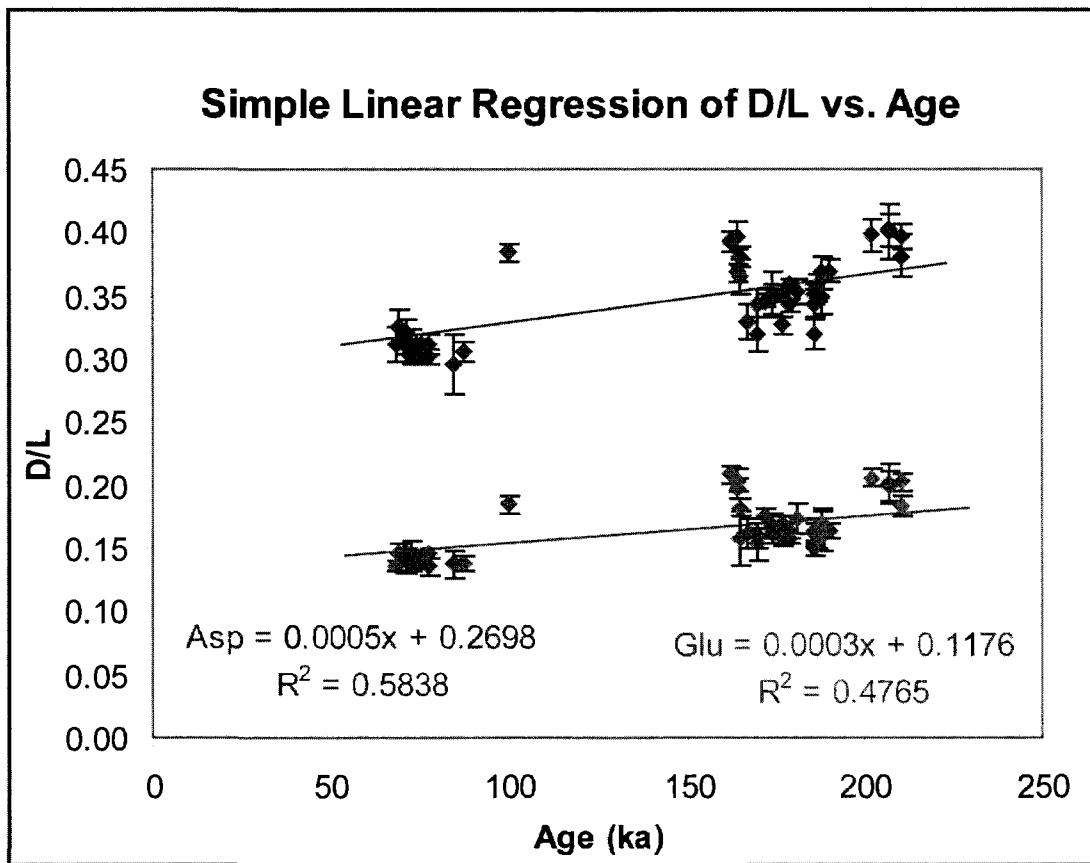
Figure 13: Simple linear regression model of D/L vs. age. All screened *Candona* and *Limnocythere* data are included in the plot. Mean D/L values were calculated by solving linear equations for values corresponding to 208 ka, 180 ka, and 74 ka.

29
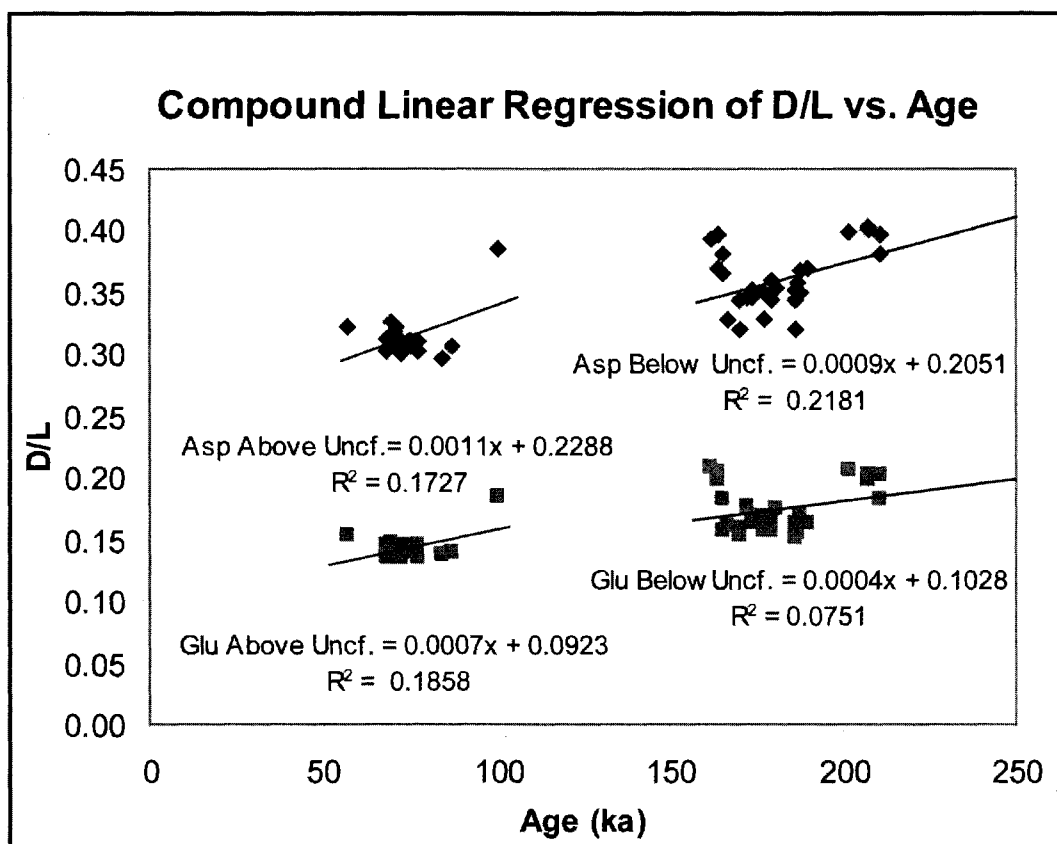
Figure 14: Compound linear regression model of D/L vs. age. All screened *Candona* and *Limnocythere* data above and below the unconformity are included in the plot. Using a compound model takes into account the potential effects of missing time due to the presence of the prominent unconformity.

3.3 Paleotemperature estimation

Four estimates of EDT were calculated from each method for deriving mean D/L values, including: (1) T_1 = EDT since the deposition of the younger sample; (2) T_2 = EDT since the deposition of the older sample; (3) $T_{(t2-t1)}$ = EDT of a time interval bracketed by t_1 and t_2; and (4) ΔT = the difference in EDT between $T_{(t2-t1)}$ and T_1 (Table 4). Overall, EDT results derived from all three approaches for determining the D/L of the bracketing ages agree within 1σ uncertainty for Asp and Glu. Glu-derived estimates of $T_{(t2-t1)}$ and ΔT were generally colder than Asp-derived estimates by as much as $1.3^\circ C$. The weighted mean of Asp and Glu $T_{(t2-t1)}$ estimates for all three models also agree within

the uncertainties determined by the Monte Carlo simulations (Table 3). Weighted mean

EDT estimates from Asp and Glu were determined by weighting the mean by the inverse

of their variance (Table 4).

Age (ka)	D/L estimation method	Asp D/L	Glu D/L
74 ± 2	Cluster of 9 samples	0.302 ± 0.002	0.138 ± 0.001
74 ± 2	Simple regression	0.307 ± 0.010	0.140 ± 0.008
74 ± 2	Compound regression	0.310 ± 0.009	0.144 ± 0.006
180 ± 6	Cluster of 16 samples	0.352 ± 0.003	0.163 ± 0.002
180 ± 6	Simple regression	0.360 ± 0.010	0.171 ± 0.008
180 ± 6	Compound regression	0.367 ± 0.011	0.175 ± 0.009
208 ± 10	Cluster of 5 samples	0.403 ± 0.006	0.207 ± 0.006
208 ± 10	Simple regression	0.374 ± 0.010	0.180 ± 0.008
208 ± 10	Compound regression	0.392 ± 0.011	0.191 ± 0.009

Table 3: Summary of D/L determination methods for EDT calculation. Uncertainty estimates for cluster-derived D/L are the higher of either the average internal or external error measurements on weighted grand mean D/L values (Bevington and Robinson, 2003). Uncertainties in D/L derived from the simple linear regression model are based on 1σ averages for all sample D/L values between 211 ka and 57 ka weighted by the inverse of their variance. Uncertainties in D/L derived from the compound linear regression model are based on the 1σ averages for all sample D/L values between 211-162 ka and between 100-57 ka weighted by the inverse of their variance.

EDT estimates for T_{t1}, $T_{(t2-t1)}$ and ΔT for the three methods yield results within 1σ

error for the intervals between 180 ka and 74 ka and from 74 ka to present (Table 4). In

addition, EDT estimates derived from the cluster method and compound linear regression

method are within 1σ error for the interval from 208 ka to 180 ka, although there is less

agreement with EDT estimated using the simple linear regression approach for this same

time period.

D/L$_1$	t$_1$ (ka)	D/L$_2$	t$_2$ (ka)	T$_1 \pm 1\sigma$ (°C)	T$_2 \pm 1\sigma$ (°C)	T$_{(t2-t1)} \pm 1\sigma$ (°C)	ΔT $\pm 1\sigma$ (°C)
Asp EDT from cluster-derived D/L							
0.302 ± 0.002	74 ± 2	0.352 ± 0.003	180 ± 6	1.7 ± 1.7	-0.4 ± 1.7	-2.8 ± 1.8	-4.6 ± 0.6
0.352 ± 0.003	180 ± 6	0.403± 0.006	208 ± 10	-0.4 ± 1.7	1.2 ± 1.7	6.4 ± 3.6	6.8 ± 3.2
Glu EDT from cluster-derived D/L							
0.138 ± 0.001	74 ± 2	0.163 ± 0.002	180 ± 6	3.7 ± 1.7	0.6 ± 1.7	-3.6 ± 1.8	-7.3 ± 0.6
0.163 ± 0.002	180 ± 6	0.207 ± 0.006	208 ± 10	0.6 ± 1.7	2.3 ± 1.8	7.7 ± 3.7	7.1 ± 3.4
Asp and Glu weighted mean and 1σ EDT from cluster-derived D/L							
---	74 ± 2	---	180 ± 6	2.7 ± 1.2	0.1 ± 1.2	-3.2 ± 1.3	-5.8 ± 1.4
---	180 ± 6	---	208 ± 10	0.1 ± 1.2	1.7 ± 1.2	7.0 ± 2.6	6.9 ± 2.3
Asp EDT from simple linear regression							
0.307 ± 0.010	74 ± 2	0.360 ± 0.010	180 ± 6	2.0 ± 1.8	-0.1 ± 1.7	-2.2 ± 2.3	-4.2 ± 1.9
0.360 ± 0.010	180 ± 6	0.374 ± 0.010	208 ± 10	-0.1 ± 1.7	-0.2 ± 1.8	-0.8 ± 5.4	-0.7 ± 5.2
Glu EDT from simple linear regression							
0.140 ± 0.008	74 ± 2	0.171 ± 0.008	180 ± 6	3.7 ± 1.8	1.1 ± 1.8	-2.2 ± 2.8	-5.9 ± 2.6
0.171 ± 0.008	180 ± 6	0.180 ± 0.008	208 ± 10	1.1 ± 1.8	0.8 ± 1.8	-0.9 ± 5.9	-2.0 ± 5.9
Asp and Glu weighted mean and 1σ EDT from simple linear regression							
---	74 ± 2	---	180 ± 6	2.8 ± 1.3	0.5 ± 1.2	-2.2 ± 1.8	-4.8 ± 1.5
---	180 ± 6	---	208 ± 10	0.5 ± 1.2	0.3 ± 1.3	-0.9 ± 4.0	-1.3 ± 3.9
Asp EDT from compound linear regression							
0.310 ± 0.009	74 ± 2.	0.367 ± 0.011	180 ± 6	2.1 ± 1.8	0.2 ± 1.8	-1.6 ± 2.3	-3.8 ± 1.8
0.367 ± 0.011	180 ± 6	0.392 ± 0.011	208 ± 10	0.2 ± 1.8	0.7 ± 1.8	2.7 ± 5.2	2.5 ± 5.2
Glu EDT from compound linear regression							
0.144 ± 0.006	74 ± 2	0.175 ± 0.009	180 ± 6	4.0 ± 1.8	1.3 ± 1.8	-2.0 ± 2.8	-6.0 ± 2.4
0.175 ± 0.009	180 ± 6	0.186 ± 0.009	208 ± 10	1.3 ± 1.8	1.2 ± 1.8	0.3 ± 5.8	-1.0 ± 5.8
Asp and Glu weighted mean and 1σ EDT from compound linear regression							
---	74 ± 2	---	180 ± 6	3.2 ± 1.3	0.8 ± 1.3	-1.8 ± 1.8	-4.5 ± 1.4
---	180 ± 6	---	208 ± 10	0.8 ± 1.3	0.9 ± 1.3	1.6 ± 3.9	0.9 ± 3.9

Table 4: EDT results from Summer Lake, Oregon. EDTs are estimated using the grand mean age and grand mean D/Lvalues as determined by three methods described in section 3.2.

The EDT since 74 ka ranges between 2.7 ± 1.2°C and 3.2 ± 1.3°C among the three methods. There is a range of EDT estimates since 180 ka between 0.1 ± 1.2°C and 0.8 ± 1.3°C (Table 4). The estimated EDT for the period spanning 208 ka to present is between 0.3 ± 1.3°C and 1.7 ± 1.2°C. EDTs shown in Figure 15 are weighted mean T$_1$ estimates derived from Asp and Glu data. EDT results between 208-180 ka estimated using the clustered D/L method are not in agreement with EDTs estimated using the simple linear regression-derived D/L values for the same interval of time. The clustered D/L method results in an EDT of 7.0 ± 2.6°C for the interval from 208-180 ka, which

spans from late MIS 7 to the middle of MIS 6 (Figure 16; Table 4). Between 180-74 ka the estimated EDT is between -1.8 ± 1.8°C and -3.2 ± 1.3°C (Table 4).
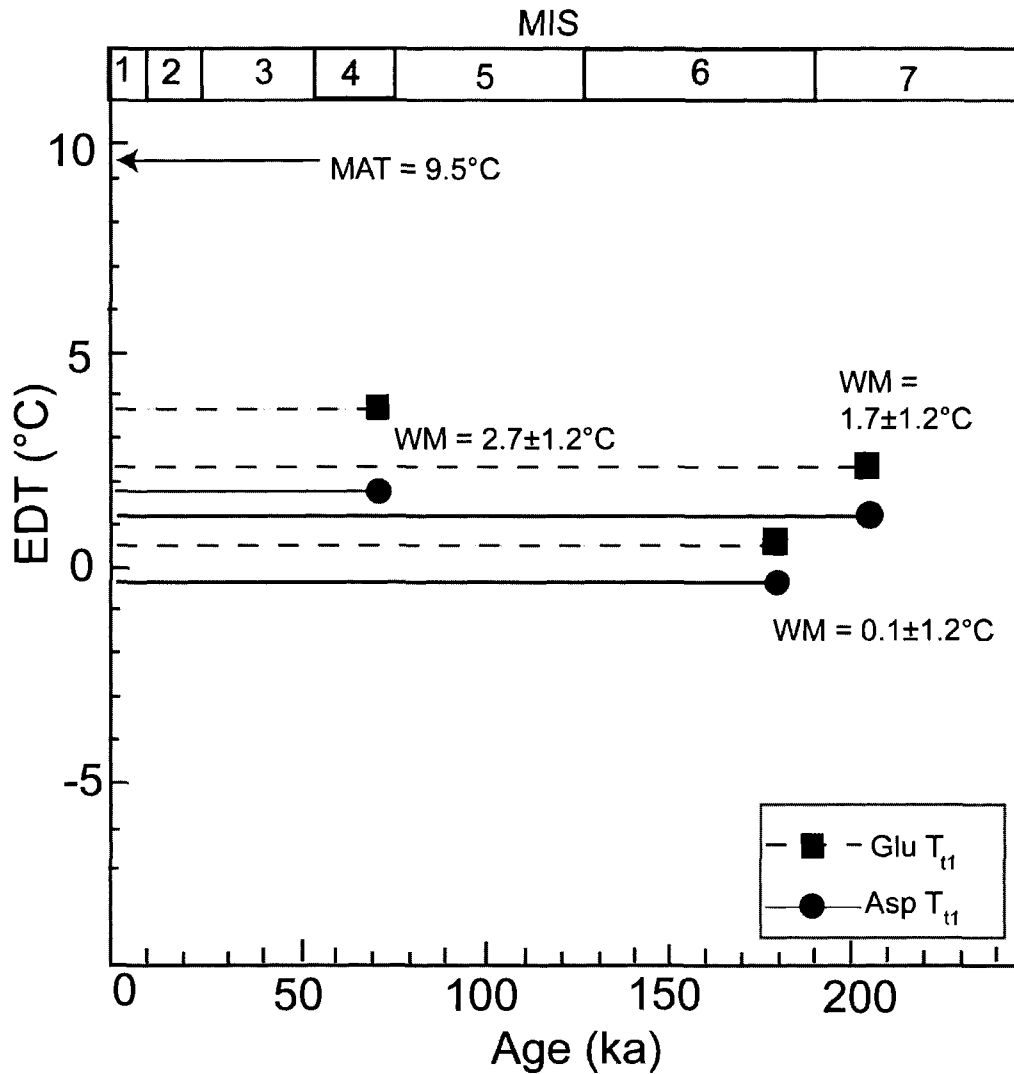
Figure 15: EDTs since time of burial by cluster approach. Plot shows cluster-derived EDT estimates for intervals since time of sample burial to present-day from 208, 180, and 74 ka, respectively. Glacial MIS are shown in grey.
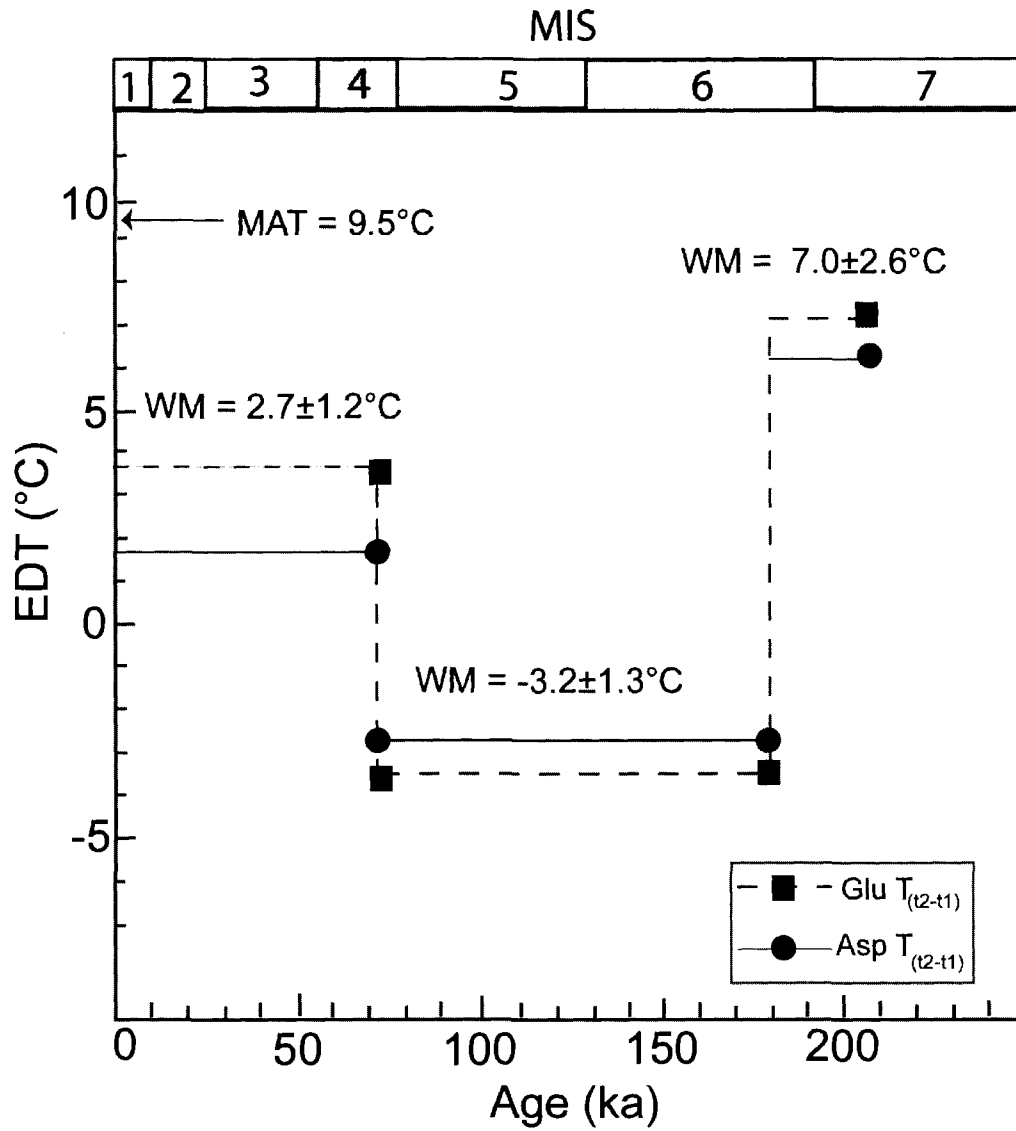
Figure 16: EDTs for bracketed time intervals by cluster approach. Plot shows cluster-derived EDT estimates for time intervals bracketed between 208, 180, 74 ka, and present-day. Glacial MIS are shown in grey.

CHAPTER 4

DISCUSSION

4.1 Evidence for taxonomic effects on racemization

A taxonomic effect on D/L values was identified in the Ana River section between *Candona* and *Limnocythere* ostracodes, with *Limnocythere* showing faster rates of racemization. This specific taxonomic effect is unique to the Summer Lake basin, as the AAR data from the Bonneville basin were insufficient to detect a consistent taxonomic effect. The average ratio of $D/L_{Candona}$ to $D/L_{Limnocythere}$ from Lake Bonneville samples is 1.05 ± 0.13 for Asp and 1.12 ± 0.18 for Glu, which compares to 0.909 ± 0.010 for Asp and 0.936 ± 0.009 for Glu from the Summer Lake basin. Kaufman (2003a) concluded that the difference in racemization rate between these two genera in the Lake Bonneville basin was not significant because the standard deviation of each ratio was high in relation to the ratio itself. In comparison, the standard deviations of the $D/L_{Candona}$ to $D/L_{Limnocythere}$ ratios are an order of magnitude smaller in the Ana River section samples, which suggests that *Candona* racemize significantly slower than *Limnocythere* in the Summer Lake basin. Evidence of a significant taxonomic effect on racemization between *Limnocythere* and *Candona* in the Ana River section is further substantiated by the fact that the 95% confidence intervals of the least squares regression

35

fit of *Limnocythere* D/L vs. *Candona* D/L do not overlap with the 1:1 relation between these species (Figure 12).

4.2 Interpretation of EDT results

EDTs reported here are among a small number of quantitative paleotemperature records that span MIS 6-4 in the western U.S, and are the first to isolate temperature of the MIS 7/6 transition in the Great Basin. Although EDTs were calculated using D/L values derived from three separate methods (see section 3.3), EDTs from the weighted mean-cluster approach are considered the most robust. D/L values derived from each method yielded sub-zero centigrade EDTs for the period between 180-74 ka; however, EDTs estimated using the weighted mean cluster approach from 207-180 ka are more congruent with EDT estimates from an overlapping time period in the Bonneville basin. The weighted mean-cluster approach utilizes data that exclude stratigraphic reversals in sample D/L greater than 1 σ, thus limiting the influence of outliers on group mean D/L calculations. In addition, the cluster approach has the advantage of being based on multiple samples of reliably estimated ages from a discrete sedimentary interval, which adds confidence that clusters of data are statistically significant. Using the weighted mean-cluster approach also reduces the amount of ambiguity introduced into EDT results due to the presence of the unconformity. In the discussion that follows, all interpretations of paleotemperatures in the Summer Lake basin will therefore be based exclusively on the cluster-derived EDTs (Table 4).

36

4.3 Paleoclimate interpretations and comparisons

An estimated EDT of 7.0 ± 2.6°C spanning the MIS 7/6 transition (between 208-180 ka) in the Summer Lake basin is within error of EDT estimates from the Lake Bonneville basin reported between 620-150 ka (Kaufman, 2003a) (Figure 17), adding confidence to the Summer Lake results. The Summer Lake EDT estimate of -3.2 ± 1.3°C between 180-74 ka (MIS 6-4) is approximately 6°C colder than similar-age sediments in the Lake Bonneville basin (Figure 16). Additionally, because EDTs for a given interval of time are higher than corresponding mean temperatures (Figure 8), Summer Lake data imply that mean temperatures were even colder than -3.2°C between MIS 6 and MIS 4, which would be unreasonable given that this period spans an interglacial (MIS 5e). An EDT of 2.7 ± 1.2°C from 74 ka to present in the Summer Lake basin is within error of the 4.1 ± 1.3°C (Kaufman, 2003a) and 3.0 ± 3.0°C (McCoy, 1987) EDT estimates in the Lake Bonneville basin from 150 ka to present. Additionally, in comparison to the Summer Lake EDT record since MIS 4, EDTs in the Bonneville basin between MIS 5 and MIS 1 have integrated an additional interval of warm temperatures into the thermal history resulting in expectedly warmer EDTs. This adds confidence that the Summer Lake EDT results since 74 ka are reliable. The difference in EDT between the 180-74 ka interval and the 74 ka to present interval is 5.8 ± 1.4°C (Table 4), which is likely the result of non-climate influences on the EDT results for the 180-74 ka interval.

Despite the uncertainties associated with EDT estimates from this study, the results refine understanding of the thermal history of the pluvial lake Chewaucan basin and contribute to an understanding of past temperatures in the western U.S. over the past 207 kyr. The EDT estimates spanning the MIS 7/6 transition in Summer Lake are

37

broadly consistent with other paleoclimate indices from pluvial Lake Chewaucan, most notably with a pollen-based air temperature record of cold conditions during this interval (Cohen et al., 2000). The Summer Lake EDT between 208-180 ka is also broadly consistent with pluvial Lake Chewaucan becoming fresher during this time period, potentially due to a decrease in evaporation under colder temperatures, as indicated by the ostracode salinity index (Sr/Ca) and ostracode paleoecology (Cohen et al., 2000) (Figure 5). In a broader regional context, there is some disagreement among the few other terrestrial records for temperatures during this time period, although most indicate a very cold MIS 6 through MIS 2 in the western U.S. (Table 1). For example, Quade et al. (2003) and Roberts et al. (1997) estimate that MIS 6 temperatures were approximately 10-15°C cooler than modern MAT in southern Nevada and in Death Valley (Table 1). Despite the temperature gradient between these locations and Summer Lake, these temperature depression estimates may support generally cooler but not necessarily sub-zero centigrade Summer Lake EDTs spanning MIS 6 to MIS 4.
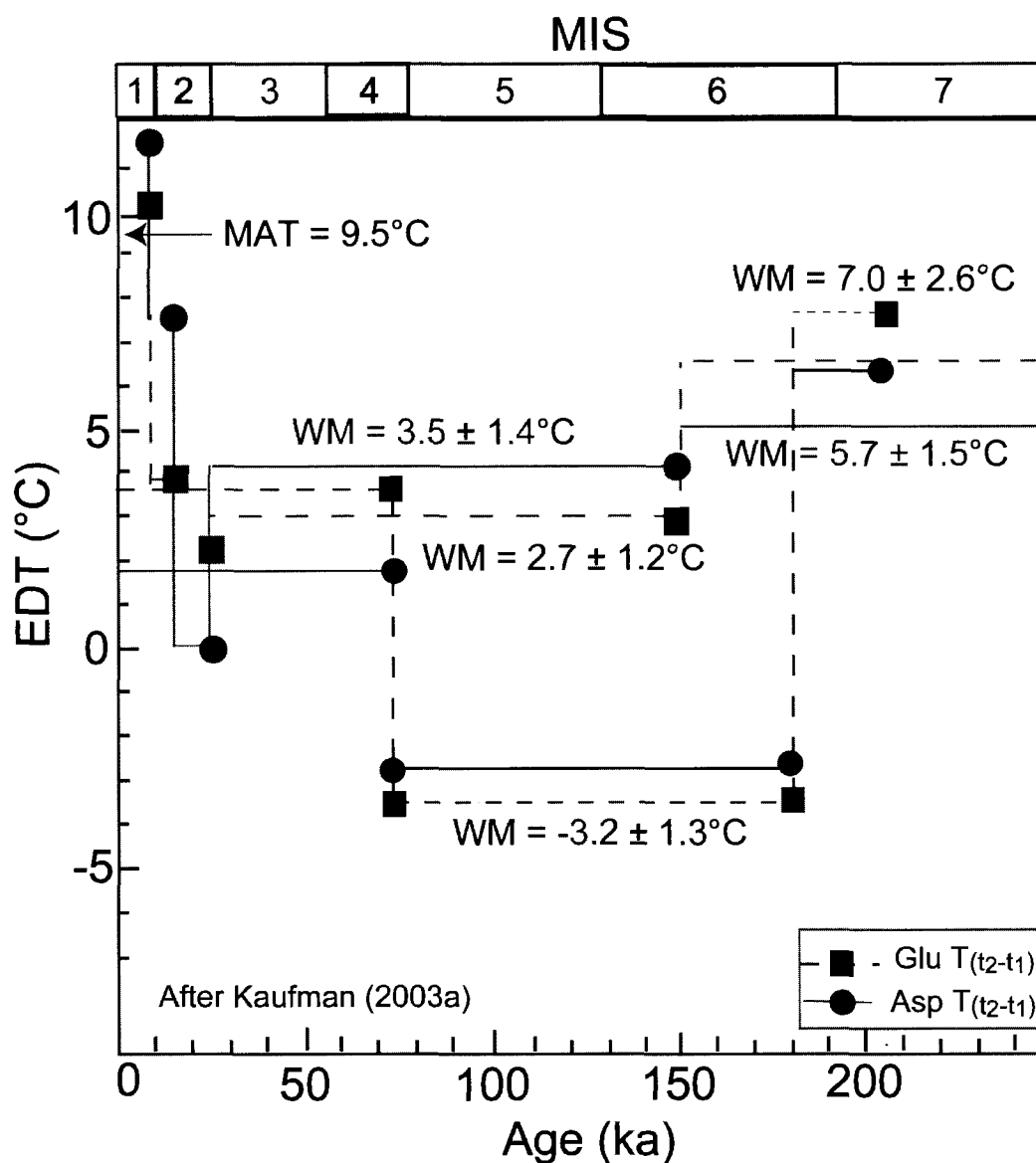
Figure 17: Comparison between Summer Lake and Lake Bonneville EDTs. EDT results from the Summer Lake and Lake Bonneville basins are in black and blue, respectively. EDT estimates from the Bonneville basin extend to 620 ka. MAT of 9.5°C shown on the figure is for the Summer Lake basin, whereas MAT in the Bonneville basin is 9.4°C. Glacial MIS are shown in grey.

It is unlikely that realistic climate forcings can fully explain sub-zero EDTs in the Summer Lake basin between 180 and 74 ka. I postulate that colder conditions in the Summer Lake basin than in the Bonneville basin from MIS 6 to MIS 4 may in part be a consequence of pluvial Lake Chewaucan's proximity to the Laurentide and Cordilleran

ice sheets. Global atmospheric circulation models show that the presence of the Laurentide Ice Sheet may have contributed to anticyclonic air flow over western North America (Manabe and Broccoli, 1985; Hostetler and Clark, 1997), which would have driven cold air toward the northern Great Basin. However, it is important to note that the anticyclone would not be present without an ice sheet , therefore the sub-zero centigrade EDTs spanning the last interglacial cannot be explained by these ice sheet-driven atmospheric circulation patterns.

At face value, the anomalously low EDT from 180-74 ka is simply a reflection that the extent of racemization changed little during this ~100 kyr period. Assuming that the D/L values measured on ostracodes are reliable, this suggests that either the change in racemization occurred on a shorter timescale than estimated by the age control used in this study (Negrini et al., 2000), or that EDTs have been overprinted by factors other than air temperature. In order to fully understand the thermal history of the Summer Lake basin, both of these considerations are explored below.

4.4 Age control uncertainties

Accurate age control for amino acid based temperature reconstruction is paramount, as equations 1 and 2 can solve for either temperature or time as the dependent variable. Given that I have confidence in the reliability of the D/L measurements, the accuracy of age control for the Ana River section is the largest potential source of uncertainty in EDT results. As mentioned in Chapter 1, the Negrini et al. (2000) age model contains multiple conflicting age estimates for the same tephra layers below the unconformity and age control is sparse between 2 m and 5 m depth above the unconformity. In addition, the timing of the unconformity is assumed to correspond to MIS 5e; however, the age of the

40

unconformity as well as the duration of subsequent basin desiccation and deflation are not well constrained.

The small amount of change in D/L values between the 180-74 ka suggests that the age for one or both D/L clusters may be inaccurate, in which case the duration of time bracketing these D/L values may actually be shorter. Therefore, overestimating the length of time between the older and younger D/L values based on an erroneous chronology could have resulted in sub-zero centigrade temperatures spanning the last interglacial.

I performed a sensitivity test to investigate the effect of varying MIS 6 and MIS 4 cluster ages on EDT. Results show that EDTs of 0.0°C can be obtained by increasing the age of the younger (MIS 4) cluster age by ~55 kyr or by decreasing the age of the older (MIS 6) cluster age by ~55 kyr. In other words, temperatures of 0.0°C or higher can be obtained if the age difference between the older and younger cluster ages is less than ~50 kyr. In either scenario, the increase or decrease in cluster age required to yield non-negative EDTs is more than the 1σ uncertainty estimated in the Negrini et al. (2000) age model based on the uncertainties of each method used to date individual horizons. This implies that revisions to the Ana River section chronology may be needed in order to better constrain EDTs in the Summer Lake basin.

4.5 Climate signal overprinting

4.5.1 Limnologic processes

Although age control uncertainty is the most probable explanation for the apparently slight change in racemization rate from 180-74 ka in the Summer Lake basin,

it is also important to consider this anomalous rate change in the context of evolving limnologic processes on millennial time scales. Thermally stratified lakes experience less than ±1°C change in seasonal water temperature below the thermocline (approximately 50 m of water) (Ragotzkie, 1978; Kaufman, 2003b and references therein). Because water temperature below a thermocline is consistently 4°C, or the temperature of the maximum density of water, fossils residing beneath the thermocline for the entirety of their depositional history are insulated from climate effects and do not record fluctuations in regional temperature in their racemization rates (Hondzo and Stefan, 1991; Kaufman, 2003b). EDT results from this study in conjunction with sedimentary evidence of shallow water facies above the unconformity indicate that the Ana River section sediments were not consistently beneath a thermocline in pluvial Lake Chewaucan over the past 208 kyr; however, they do reveal a potentially complex thermal history within the lake itself.

It is uncertain if pluvial Lake Chewaucan was thermally stratified; however, given the proximity of the Ana River outcrop to Pleistocene paleoshorelines (Figure 2) and a water depth of 90 m above the top of the Ana River section during the maximum late Pleistocene highstand (Allison, 1982), it is possible that the Ana River sediments were periodically located beneath a thermocline. Grain size analysis of pluvial Lake Chewaucan serves as a proxy for lake depth (Figure 5) and shows variable but deep lake levels through MIS 6, with a shallowing of the lake occurring from MIS 5 to MIS 2 (Erbes, 1996; Cohen et al., 2000). This is supported by field observations of clay dominated horizons below the unconformity and distinctly more sand and ooid rich strata above the unconformity (Appendix C).

4.5.2 Prolonged subaerial exposure

Because of the temperature sensitivity of the racemization reaction, D/L values are affected disproportionately by high-amplitude temperature fluctuations. D/L measured in samples collected from the top 1-2 m of the section may therefore reflect seasonal temperature fluctuations (Wehmiller, 1978; Miller and Brigham-Grette, 1989). Modern climate data from the Summer Lake basin indicate that monthly temperatures extremes fluctuate between 10°C in winter months and 20°C in summer months (Figure 4). The anomalously high D/L results for AR07-4 and AR07-6, in addition to the >3σ reversal in D/L values from AR07-6 to the next-deepest sample indicates a long duration of seasonal effects on racemization (Figure 13). For this reason, D/L results from AR07-4 and AR07-6 were excluded from all EDT calculations (Appendix D, Table A-1).

The presence of the unconformity attests to the occurrence of prolonged subaerial exposure during MIS 5, during which lake desiccation may have endured for as long as 50 ± 30 kyr based on dated tephras above and below the unconformity. Without the insulating effect of water in pluvial Lake Chewaucan, sediments now found less than 1-2 m below the unconformity during MIS 6 may have experienced large subaerial temperature fluctuations resulting in elevated D/L values. On the other hand, the sub-zero EDTs calculated for the time period spanning 180-74 ka are not easily explained unless the sediments were exposed to sustained and extremely cold temperatures in a subaerial environment during a prolonged period of lake desiccation. However, given that the emergence of the Ana River sediments occurred during the presumably warm last interglacial, it is deemed unlikely that sub-zero EDTs are the result of sustained frigid air temperatures during subaerial exposure of the Ana River sediments. This inference is

43

further substantiated by anomalously high D/L values in samples collected from 0.46 m to 1.01 m below the unconformity (Figure 12), a result which is interpreted to reflect the influence of seasonal heating on samples buried ≤1 m below the exposed ground surface during portions of MIS 5.

4.5.3 Fossil reworking and species effects

Uncertainty in the EDT estimates arising from reworking of older fossils into younger sediments is considered minimal. Although all of the untreated bulk sediment samples collected throughout the Ana River section contained some valves with clear signs of reworking, the sub-samples selected for D/L analyses in this study did not show physical evidence of reworking under a microscope. Screening of sub-sample D/L data prior to EDT calculation ensured rejection of outliers in the data that could have been the result of possible reworking. The only samples that show elevated D/L values as possible evidence of reworking are the samples collected from <1m below the unconformity lag deposit which showed a significant stratigraphic reversal in D/L values. In addition, the taxonomic effect between *Limnocythere* and *Candona* has been accounted for and is not considered a major source of uncertainty, as a sufficient number of co-occurring *Limnocythere* and *Candona* were used normalize *Limnocythere* D/L values and EDTs calculated using only *Candona* D/L values yielded similar EDTs across all time intervals examined.

CHAPTER 5

CONCLUSIONS

This study demonstrates that quantitative paleotemperature estimates can be resolved for the Summer Lake basin in southern Oregon using the application of amino acid paleothermometry to ostracodes as applied to two different types of fossil ostracodes from the Ana River section. Analyses of 33 ostracode-bearing sediment horizons collected from the Ana River section outcrop indicate that the extent of racemization increases with depth with few stratigraphic reversals in D/L. Clusters of samples with similar mean D/L values were identified at mean ages of 208, 180, and 74 ka and provide the most reliable basis for EDT analysis within the Summer Lake basin. Alternative EDTs estimated using D/L values derived by simple and compound-linear regressions are within error of EDTs estimated using the weighted mean cluster approach. Additionally all calculated EDTs for aspartic and glutamic acid agree within error determined by Monte Carlo simulations.

The EDT estimate of $7.0 \pm 2.6°C$ between 208-180 ka overlaps with modern MAT in the Summer Lake basin and is within error of slightly cooler EDTs in the Lake Bonneville basin. Qualitative paleotemperature estimates in the pluvial Lake Chewaucan basin during the MIS 7/6 transition (Cohen et al., 2000) support a cooler climate than is estimated from Summer Lake EDT calculated in this study. In conjunction with the Lake

Bonneville EDT record, EDTs reported here are among the first to quantitatively estimate paleotemperatures spanning a portion of MIS 7-6.

A very cold EDT of -3.7 ± 1.3°C is calculated between 180-74 ka, which is unreasonable given the occurrence of the last interglacial (MIS 5e) during this interval. The unreliability of the Summer Lake MIS 6-4 EDT is further substantiated by the fact that EDTs in the Lake Bonneville basin were approximately 6°C warmer for an overlapping period of time. The unreasonably cold Summer Lake EDT result is a consequence of an apparently small difference in racemization extent between 180-74 ka. Sensitivity tests suggest that the anomalous EDT between 180-74 ka is most likely explained by uncertainties in age control for the Ana River section rather than an actual decrease in racemization rate during this time interval. The possible influence of non-climate factors overprinting the climate signal is comparatively less consequential than age-depth inaccuracies as a potential source of uncertainty in EDT results from the Summer Lake basin.

EDT estimated for the interval since 74 ka is 2.8 ± 1.2°C. This estimate is within error of EDT results from the Lake Bonneville basin for an overlapping time period and is also generally consistent with observed qualitative temperature trends in the pluvial Lake Chewaucan record from this time period (Cohen et al., 2000).

EDTs from this study are among the first to yield a quantitative thermal history for the northernmost extent of the Great Basin. In addition, data obtained in this study establish a taxonomic dependency in the rate of racemization between *Limnocythere* and *Candona* in the Summer Lake basin. *Limnocythere* in the Ana River section was found to racemize faster than *Candona* at a rate of approximately 9% faster for Asp and 7%

faster for Glu. This result is unique to the Summer Lake basin, whereas D/L results from co-occurring samples of *Limnocythere* and *Candona* in the Lake Bonneville basin did not show a taxonomic dependency. The documentation of a taxon dependency on racemization contributes to the further refinement of the AAR paleothermometry method.

LIST OF REFERENCES

Allison, I.S., 1940. Study of Pleistocene lakes of south-central Oregon. Carnegie Institute Washington Yearbook 39, 299-300.

Allison, I.S., 1982. Geology of pluvial Lake Chewaucan, Lake County, Oregon. Oregon State Monographs 11, Oregon State University Press, 79 pp.

Anderson, R.S., Betancourt, J.L., Mead, J.I., Hevly, R.H., Adam, D.P. 2000. Middle- and late-Wisconsin paleobotanic and paleoclimatic records from the southern Colorado Plateau, USA. Palaeogeography, Palaeoclimatology, Palaeoecology 155, 31–57.

Antevs, E., 1952. Cenozoic climates of the Great Basin. Geologische Rundschau 40, 94-108.

Axford, Y., Geirsdottir, A., Miller, G.H., Langdon, P.G., 2009. Climate of the Little Ice Age and the past 2000 years in northeast Iceland inferred from chironomids and other lake sediment proxies. Journal of Paleolimnology 41, 7-24.

Bacon, C. R., 1983. Eruptive history of Mount Mazama and Crater Lake caldera, Cascade Range, U.S.A. Journal of Volcanology Geothermal Research 18, 57–115.

Bartlein, P.J., Anderson, K.H., Anderson, P.M., Edwards, M.E., Mock, C.J., Thompson, R.S., Webb, R.S., Webb, T.I., Whitlock, C., 1998. Paleoclimate simulations for North America over the past 21,000 years: features of the simulated climate and comparisons with paleoenvironmental data. Quaternary Science Reviews 17, 549–585.

Benson, L.V. 1999. Records of millennial-scale climate change from the Great Basin of the western U.S. In: Clark, P.U., Webb, R.S., Keigwin, L.D., (Eds), Mechanisms of Global Climate Change at Millennial Time Scales. AGU Geophysical Monograph 112, pp.203-225.

Benson, L.V., Thompson, R.S., 1987. Lake-level variation in the Lahontan Basin for the past 50,000 years. Quaternary Research 8, 69-85.

Benson, L.V., Burdett, J.W., Kashgarian, M., Lund, S.P., Phillips, F.M., Rye, R.O., 1996. Climatic and hydrologic oscillations in the Owens Lake Basin and adjacent Sierra Nevada, California. Science 274, 746-749.

Benson, L.V., Burdett, J.W., Lund, S., Kashgarian, M., Mensing, S., 1997a. Nearly synchronous climate change in the Northern Hemisphere during the last glacial termination. Nature 388, 263-265.

Benson, L.V., Smoot, J.P., Kashgarian, M., Sarna-Wojcicki, A., Burdett, J.W., 1997b. Radiocarbon ages and environments of deposition of the Wono and Trego Hot Springs tephra layers in the Pyramid Lake sub basin, Nevada. Quaternary Research 47, 251–260.

Berger, G. W., 1991. The use of glass for dating volcanic ash by thermoluminescence. Journal of Geophysical Research 96, 705–719.

Bevington, P.R., Robinson, D.K., 2003, Data Reduction and error analysis for the physical sciences, third edition: New York, McGraw-Hill, pp.320.

Brakenridge, G.R., 1978. Evidence for a cold, dry full-glacial climate in the American Southwest. Quaternary Research 9, 22–40.

Brigham-Grette, J., Melles, M., Minyuk, P. and Scientific Party, 2007. Overview and significance of a 250 ka paleoclimate record from El'gygytgyn Crater Lake, NE Russia, Journal of Paleolimnology 37, 1-16.

Chen, F.H., Bloemendal, J., Zhang, P.Z., and Liu, G.X., 1999. An 800 ky proxy record of climate from lake sediments of the Zoige Basin, eastern Tibetan Plateau, Palaeogeography, Palaeoclimatology, and Palaeoecology 151, 307–320.

Clark, P.U., Bartlein, P.J., 1995. Correlation of late-Pleistocene glaciation in the western United States with North Atlantic Heinrich events. Geology 23, 483–486.

Cohen, A.S., 2003. Paleolimnology: The History and Evolution of Lake Systems. Oxford University Press, New York. 528pp.

Cohen, A.S., Palacios-Fest, M.R., Negrini, R.M., Wigand, P.E., Erbes, D.B., 2000. A paleoclimate record for the past 250,000 years from Summer Lake, Oregon, USA: II. sedimentology, paleontology and geochemistry. Journal of Paleolimnology 24, 151-182.

Coplen, T.B., Winograd, I.J., Landwehr, J.M, Riggs, A.C., 1994. 500,000-year stable carbon isotopic record from Devils Hole, Nevada. Science 263, 361-365.

Dansgaard, W., Johnsen, S.J., Clausen, H.B., Dahl-Jensen, D., Gundestrup, N.S., Hammer, C.U., Hvldberg, C.S., Steffensen, J.P., Svelnbjornsdottir, A.E., Jouzel, J., Bond, G. 1993. Evidence for general instability of past climate from a 250-kyr ice core record. Nature 364, 218-220

Davis, J.O., 1985. Correlation of late Quaternary tephra layers in a long pluvial sequence near Summer Lake, Oregon. Quaternary Research 23, 38-53.

Delorme, L.D., 1969. Ostracodes as Quaternary paleoecological indicators. Canadian Journal of Earth Sciences 6, 1471-1476.

Dohrenwend, J.C., 1984. Nivation landforms in the western Great Basin and their paleoclimatic significance. Quaternary Research 22, 275-288.

Erbes, D.B., 1996, Late Pleistocene lithostratigraphy of pluvial Lake Chewaucan, Oregon: implications for past climate variation. California State University, Bakersfield, M.S. thesis, pp. 108

Forester, R.M., 1983. Relationship of two lacustrine ostracode species to solute composition and salinity: implications for paleohydrochemistry. Geology 11,435-438.

Garcia, A.F., and Stokes, M., 2006. Late Pleistocene highstand and recession of a small, high-altitude pluvial lake, Jakes Valley, central Great Basin, USA. Quaternary Research 65,179-186.

Henyey, S., Lund, S.P., Schwarz, M., Keigwin, L., 1995. Paleomagnetic secular variation records from deep-sea sediments of the Blake/Bahama outer ridge (North Atlantic Ocean) during oxygen-isotope Stages 5 and 6 (70–190 ka) – further evidence for the relationship between excursions and 'normal' secular variation. EOS 76, F165.

Herrero-Bervera, E., Helsley, C.E., Sarna-Wojcicki, A.M., Lajoie, K.R., Meyer, C.E., Turin, B.E., Donnelly-Nolan, J.M., McWilliams, M.O., Negrini, R.M., Liddicoat, J.C., 1994. Age and correlation of a paleomagnetic episode in the western United States by 40Ar/39Ar dating and tephrochronology: The Jamaica, Blake, or a new polarity episode ? Journal of Geophysical Research 99, 091–24,103.

Hondzo, M.; and Steffan, H.G., 1991. Lake water temperature simulation model. Journal of Hydraulic Engineering 119, 1251-1273.

Hostetler, S.W., Clark, P.U., 1997. Climatic controls of western US glaciers at the last glacial maximum. Quaternary Science Reviews 16, 505–511.

Hovan, S. A., Rea, D. K., Pisias, N. G., and Shackleton, N. J., 1989. A direct link between the China loess and marine ^{18}O records: aeolian flux to the north Pacific. Nature 340, 296–298.

Jouzel et al. 2007. Orbital and millennial Antarctic climate variability over the past 800,000 years. Science 317. p. 793 – 796.

Kaufman, D.S. 2000. Amino acid racemization in ostracodes. In: Goodfriend, G., Collins, M., Fogel, M.L., Macko, S.A., and Wehmiller, J.F. (Eds), Perspectives in amino acid and protein geochemistry. Oxford University press, pp.145-160.

Kaufman, D.S., 2003a. Amino acid paleothermometry of Quaternary ostracodes from the Bonneville Basin, Utah. Quaternary Science Reviews 22, 899-914.

Kaufman, D. 2003b. Dating deep-lake sediments by using amino acid racemization in fossil ostracodes. Geological Society of America 31, 1049-1052.

Kaufman, D.S., and Manley, W.F., 1998. A new procedure for determining enantiomeric (D/L) amino acid ratios in fossils using reverse phase liquid chromatography. Quaternary Science Reviews 17, 987-1000.

Klein, R.T., Lohmann, K.C., Kennedy, G.L., 1997. Elemental and isotopic proxies of paleotemperature and paleosalinity: climate reconstruction of the marginal northeast Pacific ca 80 ka. Geology 25, 363–366.

Kuehn, S.C., Foit, F.F., 2007. Correlation of widespread Holocene and Pleistocene tephra layers from Newberry volcano. Quaternary International 148, 113-137.

Kutzbach, J.E, Guetter, P.J., 1986. The influence of changing orbital parameters and surface boundary conditions on climate simulations for the past 18,000 years. Journal of the Atmospheric Sciences 43, 1726-1759.

Laabs, B.J.C., Plummer, M.A., Mickelson, D.M., 2005. Climate during the last glacial maximum in the Wasatch and southern Uinta Mountains inferred from glacier modeling. Geomorphology 75, 300-317.

Licciardi, J.M. 2001. Chronology of latest Pleistocene lake-level fluctuations in pluvial Lake Chewaucan basin, Oregon USA. Journal of Quaternary Science 16, 545-553.

Licciardi, J.M., Pierce, K.L., 2008. Cosmogenic exposure-age chronologies of Pinedale and Bull Lake glaciations in greater Yellowstone and the Teton Range, USA. Quaternary Science Reviews 27, 814–831.

Lisiecki, L.E., Raymo, M.E., 2004. A Pliocene-Pleistocene stack of 57 globally distributed benthic $\delta^{18}O$ records. Paleoceanography 20, PA10003.

Manabe, S., Broccoli, A.J., 1985. The influence of continental ice sheets on the climate of an ice age. Journal of Geophysical Research 90, 2167-2190.

Martinson, D. G., Pisias, N. G., Hays, J. D., Imbrie, J., Moore, T. C., and Shackleton, N., 1987. Age dating and the orbital theory of the ice ages; development of a high-resolution 0 to 300,000-year chronostratigraphy. Quaternary Research 27, 1–29.

McCoy, W.D., 1987. The precision of amino acid geochronology and paleothermometry. Quaternary Science Reviews 6, 43-54.

Menking, K.M., Anderson, R.Y., Shafike, N.G., Syed, K.H., Allen, B.D., 2004. Wetter or colder during the last glacial maximum? Revisiting the pluvial lake question in southwestern North America. Quaternary Research 62, 280– 288.

Mifflin, M.D., and Wheat, M.M., 1979. Pluvial lakes and estimated pluvial climates of Nevada. Nevada Bureau of Mines and Geology Bulletin 94, p.57.

Miller, G.H., Clark, S.J., 2007. Amino acid dating In: Elais, S.A. (Ed.), Encyclopedia of Quaternary Science, Elsevier, pp. 41-51.

Miller, G.H.; and Brigham-Grette, J. 1989. Amino acid geochronology; resolution and precision in carbonate fossils. Quaternary International 1, 111-128.

Negrini, R.M, 2002. Pluvial lake sizes in the northwestern Great Basin throughout the Quaternary period. In: Hershler, R., Madsen, D.B, and Currey, D.R. (Eds), Great Basin Aquatic Systems History. Smithsonian Contributions to the Earth Sciences 33, pp.11-53.

Negrini, R.M.; Verosub, K.L., Davis, J.O., 1988. The middle to late Pleistocene geomagnetic field recorded in fine-grained sediments from Summer Lake, Oregon, and Double Hot Springs, Nevada, U.S.A. Earth and Planetary Science Letters 87,173-192.

51

Negrini, R.M; Davis, J.O., 1992. Dating late Pleistocene pluvial events and tephras by correlating paleomagnetic secular variation records from western Great Basin. Quaternary Research 38, 46-59.

Negrini R.M., Erbes, D.B., Faber, K., Herrera, A.M., Roberts, A.P., Cohen, A.S., Wigand, P.E., Foit, F.F., 2000. A paleoclimate record for the past 250,000 years from Summer Lake, Oregon, USA: I. chronology and magnetic proxies for lake level. Journal of Paleolimnology 24, 125-149.

Oches, E.A., McCoy, W.D., Clark, P.U., 1996. Amino acid estimates of latitudinal temperature gradients and geochronology of loess deposition during the last glaciation, Mississippi Valley, United States. Geological Society of America Bulletin 108, 892-903.

Oviatt, C.G., 1997. Lake Bonneville fluctuations and global climate change. Geology 25; 155–158

Palacios-Fest, M.R., Cohen, A.S., Ruiz, J., Blank, B., 1993. Comparative paleoclimatic interpretations from nonmarine ostracodes using faunal assemblages, trace elements, shell chemistry, and stable isotope data. In: Swart, P.K., Lohmann, K.C., McKenzie, J., Savin, S. (Eds), Climate Change in Continental Isotopic Records., AGU Geophysical Monograph 78, 179-190.

Palacios-Fest, M.R, Cohen, A.S., and Anadon, P. 1994. Use of ostracodes as paleoenvironmental tools in the interpretation of ancient lacustrine records. Revista Esanola de Paleontologia 9,145-164.

Petit et al. 1999. Climate and atmospheric history of the past 420,000 years from the Vostok ice core, Antarctica. Nature 399,429-439

Pezzopane, S.K., Weldon, R.J., 1993. Tectonic role of active faulting in central Oregon. Tectonics 12, 1140-1169.

Phillips, F.M., Campbell, A.R., Bischoff, J.L., 1994. Interstadial climatic cycles: A link between western North America and Greenland? Geology 22,1115-1118.

Quade, J., Forester, R.M., Whelan, J.F., 2003. Late Quaternary paleohydrologic and paleotemperature change in southern Nevada. In: Enzel, Y., Wells, S.G., Lancaster, N. (Eds.), Paleoenvironments and Paleohydrology of the Mojave and Southern Great Basin Deserts, Geological Society of America Special Paper 368, pp. 165–188.

Ragotzkie, R. 1978. Heat budgets of lakes. In: Lerman, A. (ed). Lakes: chemistry, geology, physics. Springer-Verlag, New York, pp.1-20.

Reheis, M. 1999. Highest pluvial lake shorelines and Pleistocene climate of the western Great Basin. Quaternary Research 52,196-205.

Roberts, S.M., Spencer, R.J., Yang, W., and Krouse, H.R., 1997. Deciphering some unique paleotemperature indicators in halite-bearing saline lake deposits from Death Valley California, USA. Journal of Paleolimnology 17, 101-130.

Russell, I.C. 1884. A geological reconnaissance in southern Oregon. U.S Geological Survey Annual Report 4, 431-464.

Schroeder, R.A., Bada, J.L., 1976. A review of the geochemical applications of the amino acid racemization reaction. Earth Science Reviews 12, 347-391.

Smith, G.I., Street-Perrott, F.A., 1983. Pluvial lakes of the western United States. In: Porter, S., (Ed.), Late Pleistocene: late Quaternary environments of the United States v.1, University of Minnesota Press, Minneapolis, pp.190–211.

Stott, L., Poulsen, C., Lund, S., Thunell, R., 2002. Super ENSO and global climate oscillations at millennial time scales. Science 297, 222-226.

Thompson, R.S., Anderson, K.H., Bartlein, P.J., 1999. Quantitative paleoclimatic reconstructions from late Pleistocene plant macrofossils of the Yucca mountain region. U.S. Geological Survey Open-File Report, 99– 338.

Wehmiller J.F., Belknap, D.F., 1978. Alternative kinetic models for the interpretation of amino acid enantiomeric ratios in Pleistocene mollusks: examples from California, Washington, and Florida. Quaternary Research 9, 330-348.

Wehmiller, J.F. 1984. Interlaboratory comparison of amino acid enantiomeric ratios in fossil Pleistocene mollusks. Quaternary Research 22, 109-120.

Wehmiller, J.F. 1993. Applications of organic geochemistry for Quaternary research-Aminostratigraphy and aminochronology, In: M. Engel and S. Macko (Eds.),Organic geochemistry, Plenum Pub. Company., pp.755-783.

Zic, M., Negrini, R.M., Wigand, P.E. 2002. Evidence of synchronous climate change across the Northern Hemisphere between the North Atlantic and the northwestern Great Basin, United States. Geology 30,635-638.

APPENDICES

APPENDIX A

SAMPLE COLLECTION AND PREPARATION

1) Sediment sample collection

1. Sampling was accomplished by inserting two broad-blade putty knifes horizontally into a chosen stratigraphic horizon so as to isolate the desired sample interval.

Figure A.1: Photo of field sampling method.

2. The putty knifes were then pulled out of the section together with the chosen strata between them. A small pallet knife was then used to discard the sides and top of the isolated sample so as to avoid contamination with surrounding strata.

3. Samples were placed into pre-labeled 1-gallon Ziplock™ storage bags.

2). Raw sediment sample pretreatment

1. Samples were weighed in 1-L stainless steel beakers to which 1 g of sodium hexametaphosphate was added as a defloculant and 2 g of sodium bicarbonate was

added as a buffer. To this mixture 1 L of boiling water was added and the mixture was gently stirred so as to not break fossil valves.

2. The beakers were covered and sealed with Parafilm™, and placed in a freezer overnight.

3. Samples were thawed and gently stirred once per day for five days to break up coagulated sediments.

4. The sample slurry was then washed with DI water through a stack of 8-inch-diameter standard stainless steel sieves of 500, 325, 250, and 150 μm. Each sample was washed until DI water draining from the sieves ran completely clear, indicating that virtually all clay-sized particles were rinsed off ostracode valves.

5. Residual ostracode-rich sample was then dried on covered 150 μm sieves in a laminar flow hood.

3. Ostracode sample preparation

1. Each sample was examined under a picking scope to identify ostracode species and evaluate valves for completeness, translucency, size, abrasion, chipping, and infilling.

2. From each sample, 50 whole, adult, unarticulated, translucent, uncoated, and clean valves were hand picked from each species present for analysis.

3. The 50 picked valves were placed in a beaker with 1 L of DI water and sonicated for 10 min. The valves were then rinsed with DI water through a 150 μm sieve and dried under a laminar flow hood.

4. The valves were placed in a test tube with 2 ml of hydrogen peroxide for 2 hr, then rinsed with DI water and dried under a laminar flow hood.

5. From the initial batch of 50 valves, the best-preserved 10 *Candona* valves per sample and 20 *Limnocythere* valves per sample were chosen as sub-samples and placed in separate sterile microreaction vials.

6. Valves were dissolved in 7 μL of 6M HCl and sealed with N_2 and placed in a 110°C oven for 6 hr. This hydrolysis step breaks down peptide chains and isolates individual amino acids.

7. Hydrolyzed solutions were dried in a desiccator and rehydrated with 4 μL of 0.01 mM L-*h*Arg pH 2.
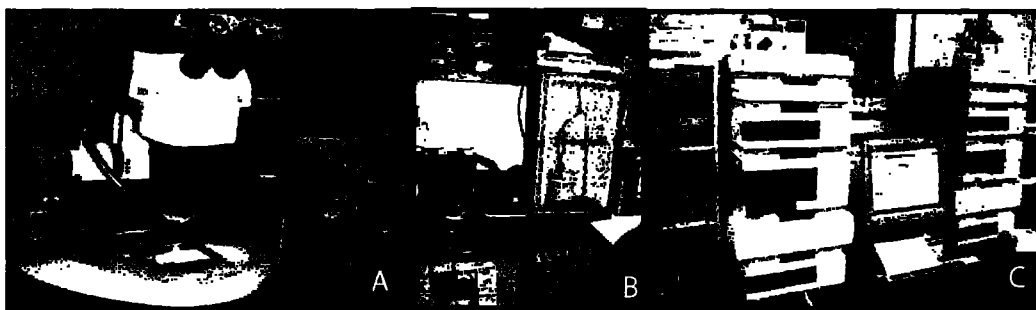
Figure A.2: Northern Arizona University amino acid geochronology laboratory. Lab is in Flagstaff, Arizona. A) picking microscope, B) ultrasonicator gently removed debris from individual ostracode valves, C) reverse-phase high performance liquid chromatograph (HPLC).

4. Instrumental Analysis

1. Sub-samples were analyzed on a Hewlett Packard HP1100 liquid chromatograph utilizing pre-column derivatization with o-phataldialdehyde (OPA), chiral thiol, and N-isobutyryl L-cysteien (IBLC) (Kaufman and Manley, 1998)..

2. As described in Kaufman and Manley (1998) the auto-injector progressively up takes 1 μL of 1 M potassium borate buffer (ph 10, 4); followed by 1 μL of 260 mM OPA/IBLC reagent; and then 1-4 μL of sample treated with 1.5 mM sodium azide ad rehydration fluid; this followed by a draw of 1 μL OPA/IBLC derivatizing reagent; then finally a draw of potassium borate buffer.

3. D- and L- amino acid enantiomers were separated using C_{18} as a stationary phase in a Hypersil BDS packed column (Kaufman and Manley, 1998).

4. Eluents A (23 mM sodium acetate with 1.5 mM sodium azide pH 6), B (methanol), and C (acetonitrille) were flushed through the column at a 1 mL/min rate at a 100%A:55%B:3%C gradient (Kaufman and Manley, 1998). D/L ratios for aspartic and glutamic acids were determined from peak areas on chromatograms.

APPENDIX B
OSTRACODE RELATIVE PERCENTAGES AND PHOTOS

□ *Limnocythere ceriotuberosa*
□ *Candona patzcuaro*
□ *Candona caudata*
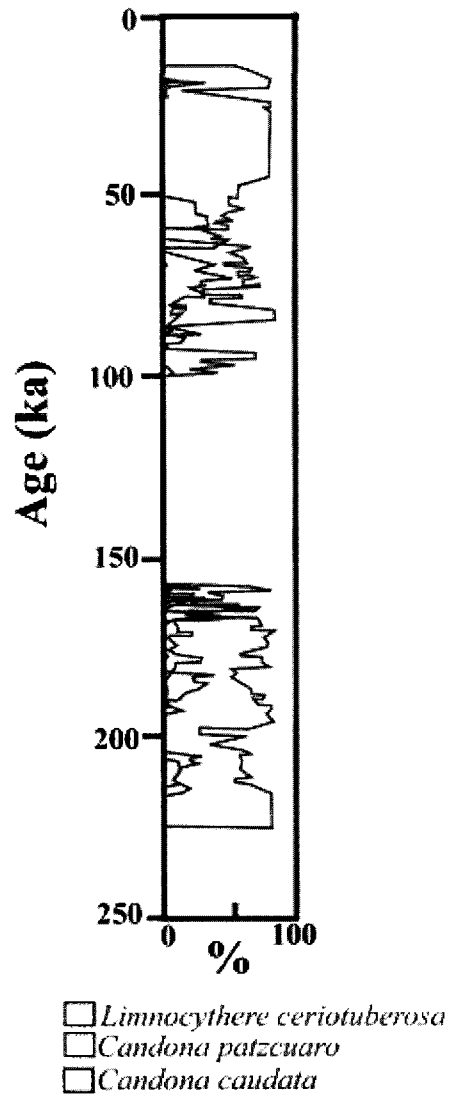
Figure A.3: Relative percentages of ostracodes in the Ana River section. Modified from Palacios-Fest et al. (1993) and Cohen et al. (2000).

courtesy of J.Bright   1.0 mm
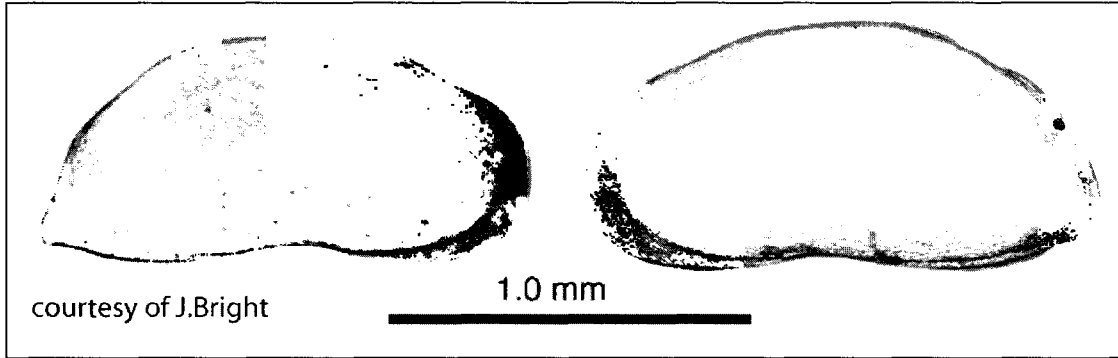
Figure A.4: *Candona sp.* 1 previously called *Candona caudata* by Palacios-Fest et al. (1993).

courtesy of J.Bright   1.0 mm
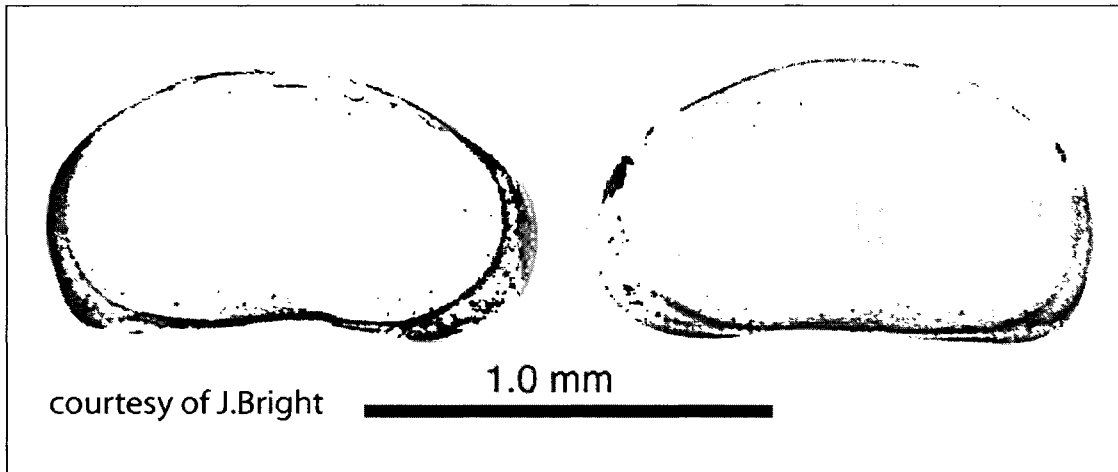
Figure A.5: *Candona sp.* 2 previously called *Candona patzcuaro* by Palacios-Fest et al. (1993).

59

Figure A.6: Male and female *Limnocythere ceriotuberosa* from the Ana River section.

APPENDIX C

ANA RIVER SECTION SEDIMENT PHOTOLOGS

m

0.00

0.10

0.20

0.30

0.40

0.50

0.60

0.70

0.80

0.90

1.00

Top of Section

Poorly sorted fine sand and silt, some pebbles

Caliche
Reverse graded fine sand silt

Caliche

Wono Tephra
Tephra G

Well sorted, laminated silt and fine sand, 2.5Y 6/3

Caliche

Mod-sorted silt and fine sand, indistinct bedding

Caliche

Caliche

Silt some clay, 10YR 5/2

Mt. St. Helen CY Ash: top 1cm is pure white ungraded, middle 6cm is v.light grey ungraded, bottom 4cm is normally graded

Med. Coarse ostracode sands interbedded with caliches

Tephra H

Caliche

Normally graded ostracode sand

Silt some clay interbedded with fine seams of sand

Grey ash

Fine to med. sand, med. brown, well sorted

Caliche

Med. Laminated fine sand and silt, abundant ostracodes, wavy bedding in bottom 7cm. 10YR 5/4

Pumice Castle: coarse grained doubly graded buff tephra. Some cross bedding.

m

2.00

2.10

2.20

2.30

2.40

2.50

2.60

2.70

2.80

2.90

3.00

Pumice Castle

Tephra 6: white ash

AR07-25: Clay

Tephra 4

Caliche

Fine sand and silt, some

Tephra 2: coarse grained ash

Finely laminated clay and silt
interbedded with thin caliches

Caliche

Reverse graded med. sand and
silt, indistinct bedding

Black seam, laterally continuous

Wavy laminations of clay and silt

Laminated silt and clay. 10YR 4/2

Coarse sand

Caliche

Laminated silt and clay. 10YR

Tephra I: lt. grey pumice

Laminated silt and clay. 10YR 4/2

Med. sand, light brown, many ostracodes

Caliche

Ooids and ostracode sand

Caliche

Tephra J: lt grey ash

Dark grayish brown clay and silt

Doubly graded med-coarse sand

Ooid sands interbedded with silt sand layers

Clay some silt, gradational contacts at base

Fine sand and silt, some clay

Tephra K: lt.grey pumice

AR07-48

m

5.00

5.10 — Finely laminated clay, grayish brown

MIS 5e unconformity: ooid beds with caliche coated ostracodes underlain by a caliche layer

5.20

Massive silty clays with root casts

5.30

5.40 — Indistinctly bedded clay intermixed with silt

Tephra P

5.50 — Tephra Q

5.60

AR07-63 — Finely laminated silty clay with pelecypod shells

5.70

Tephra R

5.80 — Oxidized silt

Indistinctly bedded clay intermixed with silt

5.90 — AR07-66

Silty clay

6.00

66

m Stratigraphy

6.00

6.10

6.20

6.30

6.40

6.50

6.60

6.70

6.80

6.90

7.00

Gastropods

0.5cm thick coarse grey ash

1.8cm thick coarse sand

Clay and silt with preserved root casts

1cm thick grey ash

Massive clay intermixed with silt

Thin beds of fine sand interbedded with clay.

Tephra R: lt.tannish grey pumice

Clay, little silt and sand. Some oxidation

Interbedded reddish-brown oxidized, thinly laminated fine sand -silt

67

m

8.00

8.10

8.20

8.30

8.40

8.50

8.60

8.70

8.80

8.90

9.00

AR07-88

AR07-89

AR07-98

Clay some silt

Ash mantled by ostracode sand

Clay some silt

Tephra X: pinkish white ash

Tephra Y and Z: black ash

Dark brown silty clay

Black seam possible ash

Dark brown silty clay

Oxidized med. sand, sharp bottom contacts

Medium sand

Ostracode sand, bedding defined by changes in color

Fine sand

69

Ostracode sand seam

Black seam

Tephra BB: Light tan ash

Silty clay

Tephra CC: normally graded white ash

Tephra DD: lt. grey ash

Tephra EE

Dark grey clay

Tephra FF

Tephra GG

Dark grey clay

AR07-122

Tephra HH: normally graded grey ash

Massive silty clay

Tephra JJ: Grey ash

Tephra JJ1: White ash

Normally grades from clay to silt to fine sand

Tephra KK

Silty clays

Ooid beds interbedded with silt beds

Clay rich silt, indistinct bedding

m

12.00 — Tephra LL: Doubly graded lt. grey ash

Clay intermixed with silt

12.10 — Tephra LL1: dark grey ash

Normally graded clay rich silt to fine sand

12.20 —

AR07-136

12.30 —

Clay mixed with silt, some fine sand, sharp basal contact

12.40 —

Ostracode sand mixed with ooids, sharp contacts

12.50 —

12.60 —

12.70 —

Silt some clay and fine sand

12.80 —

12.90 —

AR07-135

13.00 —

APPENDIX D

SUPPLEMENTAL RACEMIZATION DATA

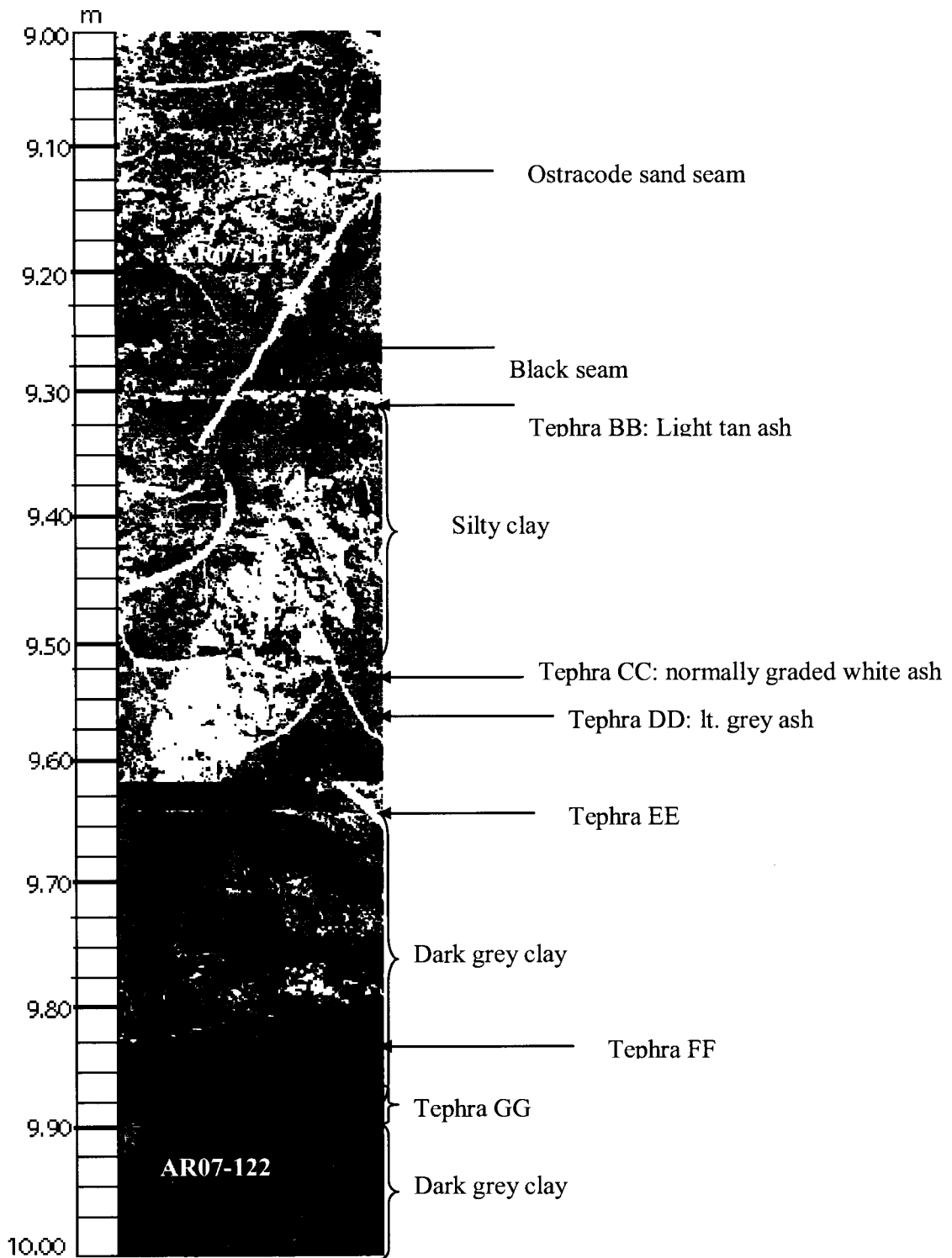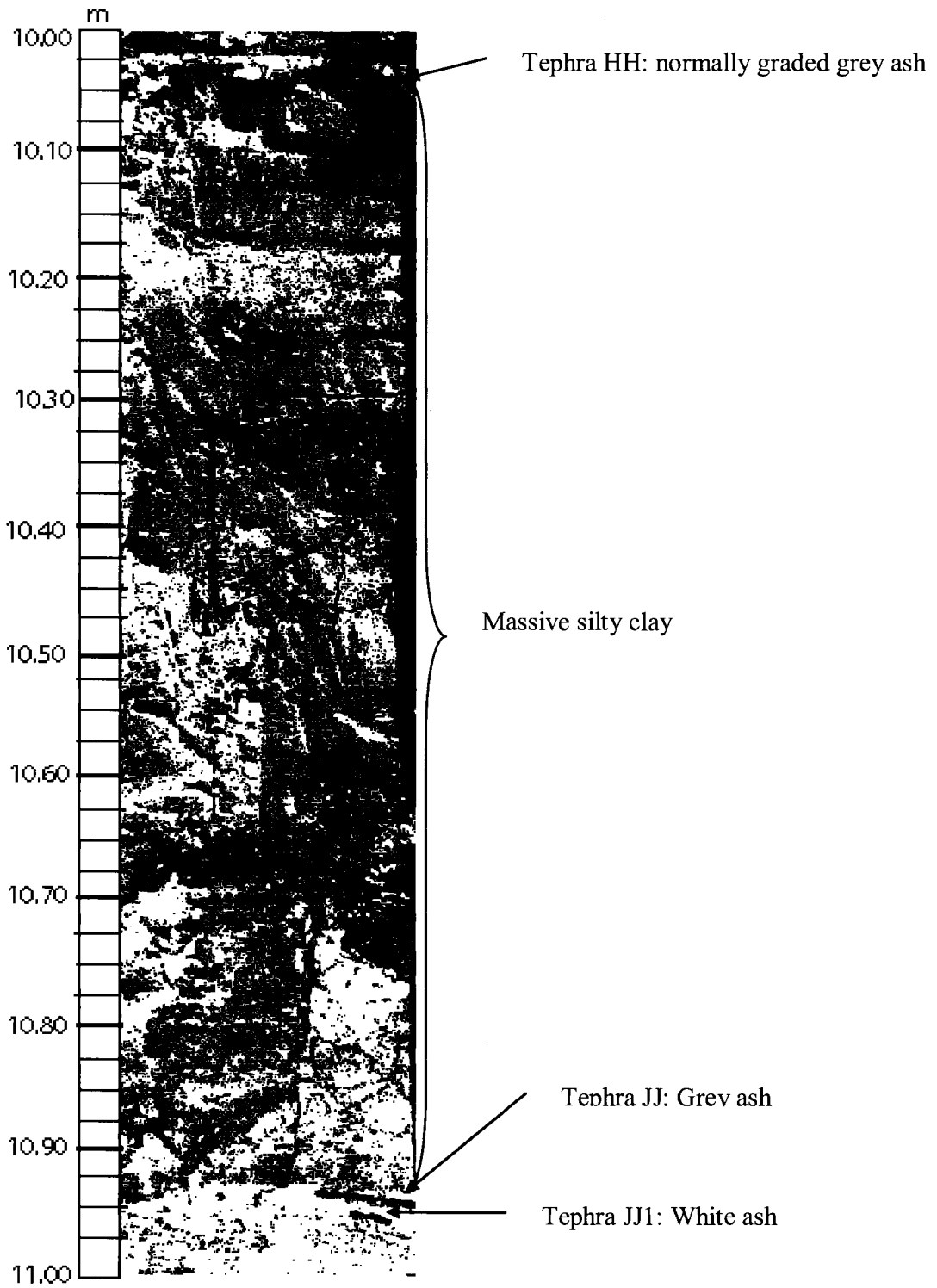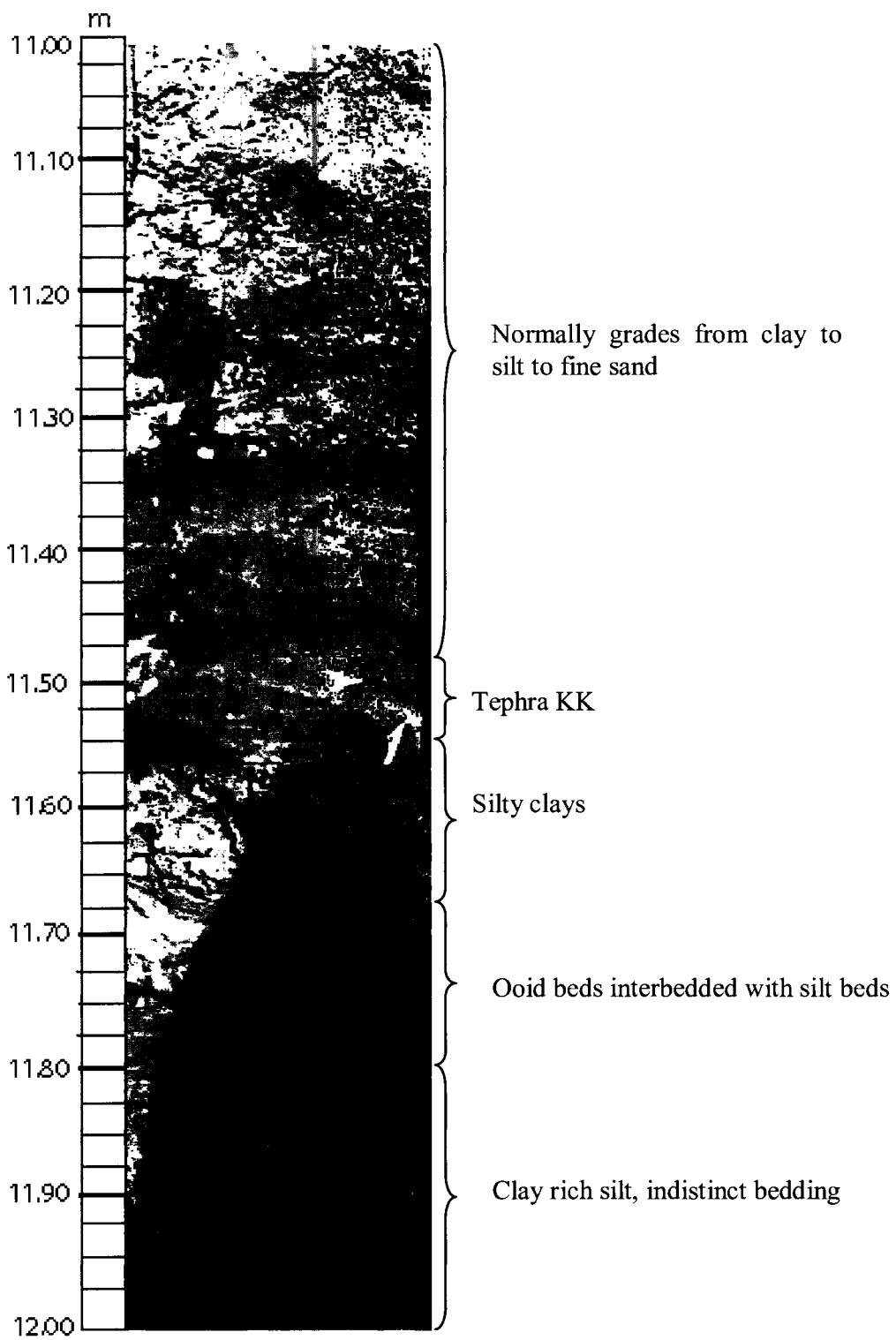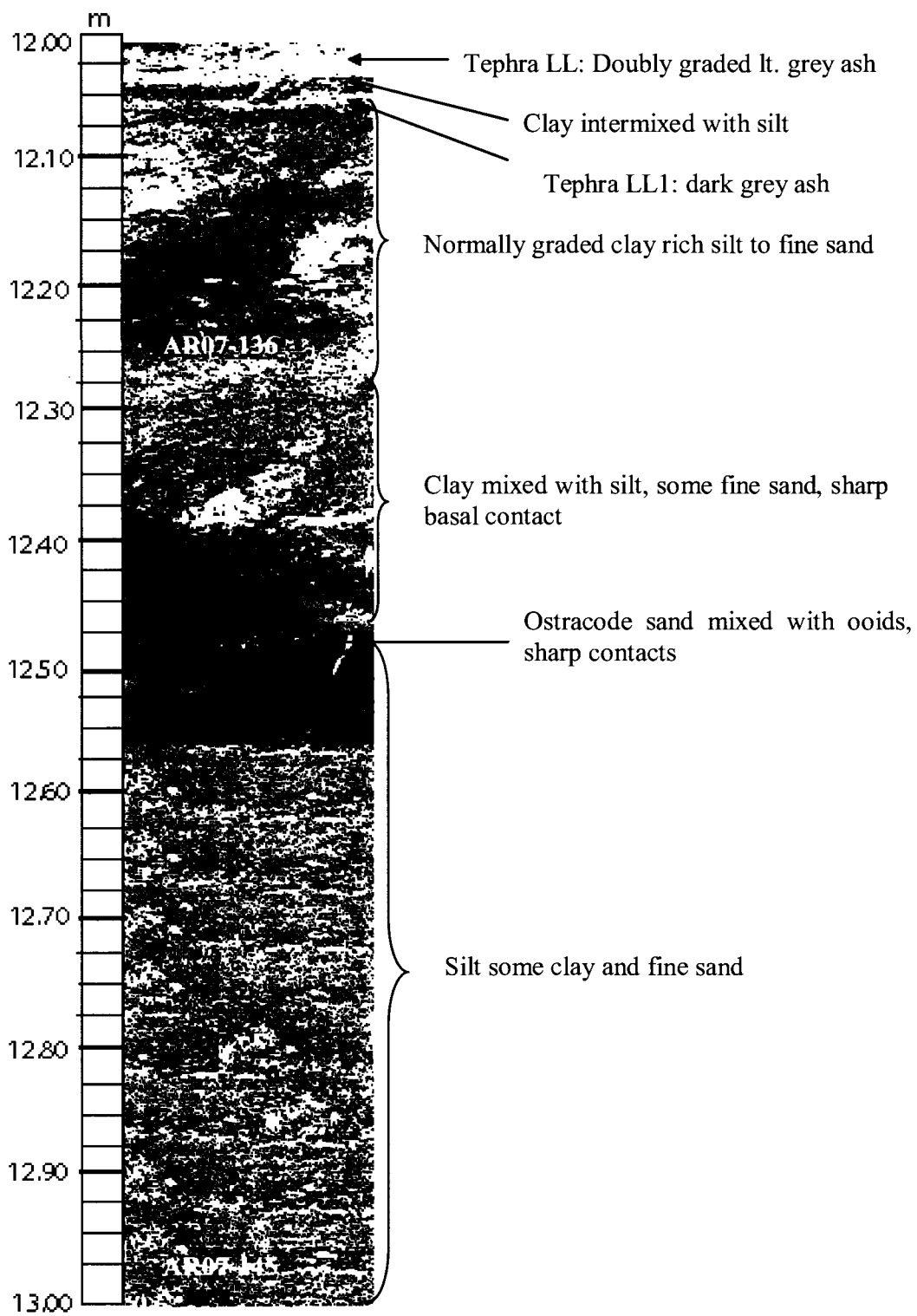| Age (ka)	Depth (m)	UAL	Sample #	species	n	ex	Unadjusted Asp D/L±σ	Adjusted Asp D/L±σ	Unadjusted Glu D/L±σ	Adjusted Glu D/L±σ
29±0.3	0.46	6789	AR07-4	*L.ceriotuberosa*	9	1	0.389±0.019	0.352 ± 0.017	0.206±0.019	0.192±0.018
32±0.5	0.58	6790	AR07-6	*L.ceriotuberosa*	10	0	0.369±0.007	0.334±0.006	0.178±0.004	0.166±0.004
57±3.0	1.47	7040	AR07-19	*C.caudata*	9	0	0.322±0.006	0.322±0.006	0.153±0.009	0.153±0.009
68±6.4	2.01	6624	AR07-23	*C.caudata*	9	1	0.302±0.008	0.302±0.008	0.145±0.010	0.145±0.010
68±6.4	2.01	6810	AR07-23	*L.ceriotuberosa*	7	3	0.334±0.014	0.303±0.013	0.137±0.004	0.127±0.004
69±6.6	2.06	6807	AR07-25	*L.ceriotuberosa*	8	1	0.353±0.014	0.320±0.013	0.152±0.007	0.141±0.007
70±6.7	2.08	6625	AR07-27	*C.caudata*	8	3	0.318±0.006	0.318±0.006	0.145±0.005	0.145±0.005
71±7.0	2.15	6627	AR07-28	*C.caudata*	8	2	0.309±0.006	0.309±0.006	0.140±0.008	0.140±0.008
71±7.0	2.15	6791	AR07-28	*L.ceriotuberosa*	9	1	0.348±0.009	0.315±0.008	0.150±0.004	0.140±0.004
72±7.2	2.25	6620	AR07-30	*C.caudata*	7	2	0.302±0.006	0.302±0.006	0.136±0.003	0.136±0.003
72±7.2	2.25	6621	AR07-30	*L.ceriotuberosa*	9	0	0.330±0.014	0.299±0.013	0.148±0.012	0.138±0.011
74±7.5	2.43	6629	AR07-33	*C.caudata*	8	1	0.310±0.010	0.310±0.010	0.139±0.005	0.139±0.005
75±7.6	2.58	7041	AR07-34	*C.caudata*	7	3	0.311±0.009	0.311±0.009	0.142±0.005	0.142±0.005
75±7.6	2.58	7083	AR07-34	*L.ceriotuberosa*	5	2	0.324±0.008	0.294±0.007	0.149±0.004	0.139±0.004
77±7.8	2.70	7042	AR07-35	*C.caudata*	8	2	0.302±0.006	0.302±0.006	0.136±0.007	0.136±0.007
77±7.8	2.70	7081	AR07-35	*L.ceriotuberosa*	5	1	0.332±0.008	0.301±0.007	0.150±0.004	0.140±0.004
84±8.7	3.35	7082	AR07-38	*L.ceriotuberosa*	5	1	0.311±0.027	0.282±0.024	0.139±0.009	0.129±0.008
87±9.1	3.65	6792	AR07-40	*L.ceriotuberosa*	7	3	0.324±0.006	0.294±0.005	0.141±0.006	0.131±0.006
100±11	4.80	6805	AR07-51	*L.ceriotuberosa*	8	2	0.438±0.006	0.397±0.005	0.207±0.007	0.193±0.007
162±23	5.52	7043	AR07-63	*C.patzcuaro*	7	2	0.393±0.009	0.393±0.009	0.208±0.008	0.208±0.008
164±23	5.80	6610	AR07-66	*C.patzcuaro*	8	1	0.398±0.011	0.398±0.011	0.204±0.008	0.204±0.008
164±23	5.80	6611	AR07-66	*L.ceriotuberosa*	6	4	0.415±0.008	0.376±0.007	0.225±0.009	0.209±0.008
165±23	6.00	6628	AR07-69	*C.patzcuaro*	6	4	0.366±0.014	0.366±0.014	0.157±0.022	0.157±0.022
165±23	6.00	6808	AR07-69	*L.ceriotuberosa*	8	2	0.433±0.009	0.392±0.008	0.203±0.007	0.189±0.007

Table A.1: Extent of aspartic and glutamic acid racemization in *Candona* and *Limnocythere*. UAL is the lab identification number for each sample, n is number of sub-samples after data screening, ex is number of sub-samples excluded. *Limnocythere* D/L values in the adjusted columns have been normalized to *Candona*.

Age (ka)	Depth (m)	UAL	Sample #	species	n	ex	Unadjusted Asp D/L±σ	Adjusted Asp D/L±σ	Unadjusted Glu D/L±σ	Adjusted Glu D/L±σ
167±23	6.26	6811	AR07-73	L.ceriotuberosa	7	3	0.358±0.011	0.324±0.010	0.174±0.011	0.162±0.010
170±23	6.86	6603	AR07-76	C.patzcuaro	7	2	0.344±0.011	0.344±0.011	0.160±0.009	0.160±0.009
170±23	6.86	6607	AR07-76	L.ceriotuberosa	8	3	0.345±0.014	0.313±0.013	0.162±0.0130	0.151±0.012
172±23	7.13	6622	AR07-78	L.ceriotuberosa	5	4	0.382±0.005	0.346±0.005	0.194±0.005	0.180±0.005
174±23	7.45	6608	AR07-82	C.patzcuaro	7	3	0.352±0.018	0.352±0.018	0.163±0.009	0.163±0.009
174±23	7.45	6609	AR07-82	L.ceriotuberosa	5	2	0.383±0.012	0.347±0.011	0.183±0.010	0.170±0.009
177±23	7.80	7044	AR07-88	C.patzcuaro	10	1	0.350±0.005	0.350±0.005	0.170±0.004	0.170±0.004
177±23	7.80	7079	AR07-88	L.ceriotuberosa	8	3	0.355±0.007	0.322±0.006	0.167±0.006	0.155±0.006
179±23	8.19	6626	AR07-89	C.patzcuaro	9	1	0.343±0.005	0.343±0.005	0.158±0.004	0.158±0.004
179±23	8.19	6793	AR07-89	L.ceriotuberosa	8	2	0.402±0.003	0.364±0.003	0.177±0.006	0.165±0.006
181±23	8.54	7045	AR07-98	C.patzcuaro	10	0	0.354±0.010	0.354±0.010	0.174±0.012	0.174±0.012
186±23	9.28	6612/13	AR07-106	Total Candona	12	1	0.351±0.008	0.351±0.008	0.164±0.010	0.164±0.010
186±23	9.30	6614	AR07-106	L.ceriotuberosa	10	1	0.395±0.009	0.358±0.008	0.173±0.006	0.161±0.006
186±23	9.30	6615	AR07-108	L.ceriotuberosa	10	1	0.386±0.011	0.350±0.010	0.161±0.006	0.150±0.006
186±23	9.30	6616/17	AR07-108	Total Candona	15	2	0.344±0.011	0.344±0.011	0.158±0.009	0.158±0.009
187±23	9.41	6618	AR07-110	L.ceriotuberosa	8	2	0.398±0.010	0.361±0.009	0.165±0.006	0.153±0.006
188±23	9.63	6623	AR07-114	C.patzcuaro	10	0	0.349±0.013	0.349±0.013	0.170±0.009	0.170±0.009
188±23	9.63	6809	AR07-114	L.ceriotuberosa	9	1	0.414±0.013	0.375±0.012	0.178±0.018	0.166±0.017
190±23	9.88	7046	AR07-122	C.patzcuaro	10	1	0.369±0.009	0.369±0.009	0.164±0.006	0.164±0.006
202±23	11.78	7078	AR07-136	L.ceriotuberosa	8	2	0.458±0.013	0.415±0.012	0.237±0.006	0.220±0.006
207±23	12.50	6630	AR07-145	C.patzcuaro	10	1	0.402±0.013	0.402±0.013	0.199±0.013	0.199±0.013
207±23	12.50	6806	AR07-145	L.ceriotuberosa	6	2	0.462±0.022	0.419±0.020	0.231±0.016	0.215±0.015
211±23	13.10	7077	AR07-148	L.ceriotuberosa	10	2	0.434±0.014	0.393±0.013	0.204±0.008	0.190±0.007
211±23	13.10	7039/47	AR07-148	Total Candona	12	3	0.398±0.010	0.398±0.010	0.202±0.007	0.202±0.007

Table A.1 continued: Extent of aspartic and glutamic acid racemization in *Candona* and *Limnocythere*. UAL is the lab identification number for each sample, n is number of sub-samples after data screening, ex is number of sub-samples excluded. *Limnocythere* D/L values in the adjusted columns have been normalized to *Candona*.